JOURNAL OF NEW ENERGY

An International Journal of New Energy Systems Vol. 1, No. 3, 1996

Published by the
Fusion Information Center
P.O. Box 58639
Salt Lake City, Utah 84158-0639

A Quarterly Journal
Subscription: $150 for 4 issues
Single issues: $45

Fall 1996

ISSN 1086-8259

NUCLEAR TRANSMUTATIONS IN THIN-FILM NICKEL COATINGS UNDERGOING ELECTROLYSIS

George H. Miley [1] and James A. Patterson [2]

ABSTRACT

Experiments using 1-mm plastic and glass microspheres coated with single and multilayers of thin films of various metals such as palladium and nickel, used in a packed-bed electrolytic cell (Patterson Power Cell ™ configuration), have apparently produced a variety of nuclear reaction products. The analysis of a run with 650-Å film of Ni is presented here. Following a two-week electrolytic run, the Ni film was found to contain Fe, Ag, Cu, Mg, and Cr, in concentrations exceeding 2 atom % each, plus a number of additional trace elements. These elements were at the most, only present in the initial film and the electrolyte plus other accessible cell components in much smaller amounts. That fact, combined with other data, such as deviations from natural isotope abundances, seemingly eliminates the alternate explanation of impurities concentrating in the film.

A 1-molar lithium sulfate solution in light water was employed for the electrolyte. A small excess heat of approximately 0.5 ± 0.4 watts was recorded throughout the run. Reaction products were analyzed using a combination of secondary ion mass spectrometry (SIMS), Auger electron spectrometry (AES), energy dispersive x-ray (EDX) analysis, and neutron activation analysis (NAA).

Results showing a broad array of products such as found here have also been obtained with thin film coatings of other materials, e.g., Pd and multi-layers of Pd and Ni. The yields of the major elements contributing depend on the film material, however. Some of that work is still being analyzed and will be presented at ICCF-6 [15].

The array of products found in these experiments is consistent with recent studies of solid Pd and Au electrodes by Mizuno et al. [19] and Ohmori and Enyo [22] , respectively. A distinct advantage of thin electrode construction used here, however, is that the reaction zone becomes well defined, enabling quantitative measurements of the amounts of various products.

To explain the observation of products with atomic numbers both well above and below Ni, a reaction model is being developed that involves proton-induced excited complexes, followed in some cases by a fission of the unstable compound nucleus

INTRODUCTION

Various nuclear transmutation products generated during electrolytic cell operation, typically employing Pd and heavy or light water with various electrolytes such as Na_2CO_3 and LiOH, have previously been reported, e.g., see the proceedings of the first conference in this series (Bockris and Lin [1]). Most of these reports have dealtwith impurity level quantities of specific elements, such as Sr, Rb or tritium, although some workers, such as Mizuno

[1] Fusion Studies Laboratory, U. of Illinois, 103 S. Goodwin Avenue,Urbana, IL 61801-2984
Ph. 217-333-3772 Fax 217-333-2906 E-mail: g-miley@uiuc. edu

[2] Clean Energy Technologies, Inc., 1 Lincoln Center, 5400 LBJ Freeway, Suite 950, Dallas, TX 75240
Ph. 972-982-8340 Fax 972-982-8349

et al.[19], Ohmori and Enyo [22] , and Karabut et al.[7] report on a wide variety of isotopes occurring at impurity levels. Several investigators, e.g., Miles and Bush [10], have concentrated on ^4He, which they view as a logical reaction product for nuclear reactions in solids.

While the occurrence of this number of independent observations strongly implies that chemically assisted nuclear reactions in solids are possible, the quantification and the credibility of the results have suffered from low, impurity-level yields and non-reproducibility. In sharp contrast, the thin (<2000Å) films used in present work result in transmutation of a significant percentage of the metal in the thin-film cathode due to the "small" number of host atoms. (While, as stressed later, impurity contributions can not be completely ruled out, the term "transmutation products" is used here due to the overwhelming evidence in favor of this identification.)

Over a dozen experiments with various types of thin-film coatings have been carried out in different cells (Miley and Patterson [17]). Thin-film coatings on 1-mm-diameter plastic/glass microspheres, ranging from 500-Å-thick single layers of Pd or Ni to multiple Ni/Pd layers, were used in a flowing packed-bed-type electrolytic cell with a 1-molar Li_2SO_4 light water electrolyte. Nuclear reaction products were obtained in all cases, with several runs resulting in over 40 atomic % of the original coating materials being transmuted to reaction products such as Fe, Si, Mg, Cu, Cr, Zn, and Ag. The present paper deals with the specific case of a single nickel thin film, since it has been analyzed most thoroughly to date and appears to be representative of the behavior observed in the other runs.

The "normal" Patterson Power Cell employs electrolytically coated layers of Ni and Pd on microspheres, and this composition has been extensively studied for power production (Patterson [24]). The Ni-coated thin film microspheres described here were developed explicitly for reaction product studies, although power production with "conventional" thick Ni electrodes in light water cells has been widely studied (e.g., see I. Myers et al. and references therein [20]).

The use of thin-film coatings originates from the "swimming electron layer" (SEL) theory proposed earlier (Hora, Miley, et al. [5]; Miley et al.[12]; Miley et al.[14]), which suggests that nuclear reactions are assisted by the use of multilayer thin films with alternating metals that have large differences in Fermi energy levels. The resulting increase in electron density at the film interface is shown to "squeeze" excess electrons between ions, greatly reducing the Coulombic barrier, thus enhancing nuclear reactions. This theory was first studied using thin-film Pd/Ti coatings sputtered onto a large stainless steel substrate electrode (Miley et al. [14]). Those experiments were terminated due to flaking of the films off of the electrode soon after loading and heating occurred. However, the results were very encouraging, since high excess heat (estimated to be kW/cm^3 at the interface regions) was observed for minutes prior to the disintegration of the thin films. Subsequently, J. Patterson [24] developed a unique electrode configuration using electrochemical deposition of relatively thick (mm) coatings of Ni/Pd layers on millimeter diameter cross-linked polymer microspheres. These microspheres were then employed in a flowing packed-bed-type electrolytic cell (Patterson Power Cell). The coatings, while thicker than the earlier thin-film studies, were found to be quite stable in this configuration, so experiments with thin films (300- to 2000-Å thick) on such microspheres were undertaken in the present work.

The thin films were laid down using a special sputtering process (Miley, Name, et al.[18]), where the microspheres are suspended in a fluidized state during the spraying process. The metallurgy of the films themselves has been studied before and after electrolysis, using both Auger electron probe techniques and electron microscopic surface analysis.

Reaction product measurements have utilized a combination of secondary ion mass spectrometry (SIMS), Energy Dispersive X-ray (EDX) analysis, Auger Electron Spectroscopy (AES), and neutron activation analysis (NAA). SIMS is used to obtain a broad view of both high and low concentration isotopes present and their isotopic ratios, while NAA provides a quantitative measure of the masses of key elements. EDX provides confirmatory data for

elements having high concentrations, while AES is used for depth-profiling of high concentration elements. NAA can obtain total quantities of elements in a sample typically containing 10 microspheres, while the other techniques are restricted to probing a local area on single microspheres. Due to variations among microspheres due to location in the packed bed and other effects, this difference in samples becomes very important in present work. The analysis techniques and the nuclear reaction products observed are described further in following sections

ELECTROLYTIC CELL DESCRIPTION AND OPERATION

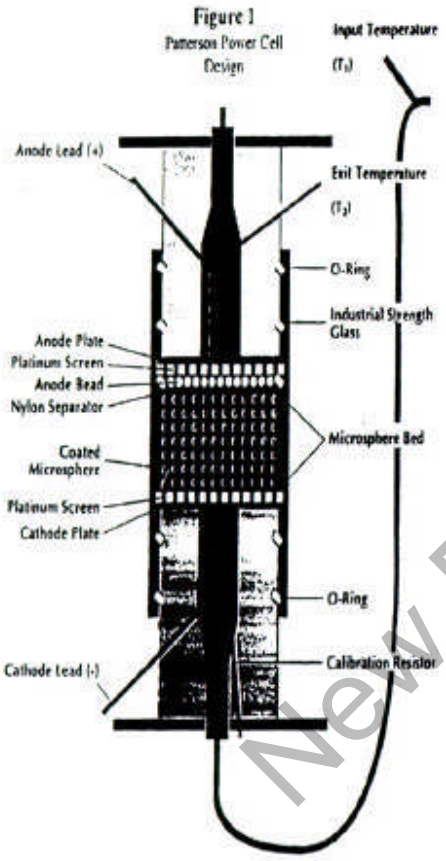

Fig. 1a. Schematic Diagram of a Patterson Cell

The general configuration of the Patterson-type electrolytic cell employed is shown in Fig. 1a. About 1000 microspheres (~0.5 cm^3 volume) were used in the packed-bed cell. Titanium electrodes were employed in the present Ni run and in most other runs, except for a few cases where Pt electrodes were used for comparison purposes.

A flow diagram is shown in Fig. 1b. A preheater allowed control of the temperature of the electrolyte entering the cell from 20-70° C, with flow rates of ~11 ml/min. Voltages across the bed were held at ~2-3 V, with several mA of current, giving an electrical input power of approximately 0.06 W. The pump and preheater consume an additional 5 W, but this input does not enter into the energy balance across the cell; hence the 5 W is not involved in the computation of excess heat production. Inlet-outlet thermocouples provide a measure of the temperature increase of the flowing electrolyte typical values ranged from 0.1 to 4° C, corresponding to about 0.1 to 4 W output, depending on the films used. Positive outputs were observed in all cases, but due to the calorimeter technique, the values are only considered to be accurate to ±0.4 W. More precise calorimetry is in use in several laboratories studying excess power from the Patterson cell, but here the cell design was focused on ease of reaction product measurement. In view of the positive results reported here, further work with improved calorimetry and periodic sampling of microspheres during runs is warranted to obtain a quantitative relation between the power (or energy production/run) and the various reaction products.

Such studies are now in progress. Still, the present reaction product data provides a first insight into this important new field of chemically-assisted nuclear reactions using thin-film electrolysis.

Loading of hydrogen into the thin film is typically done at low (25° C) temperatures and requires several hours, as observed by an initial increase in the voltage across the bed, i.e., the change in film resistance, followed by an eventual equilibrium voltage level of +2 to 3 V. The loading time, defined as the time to reach this equilibrium

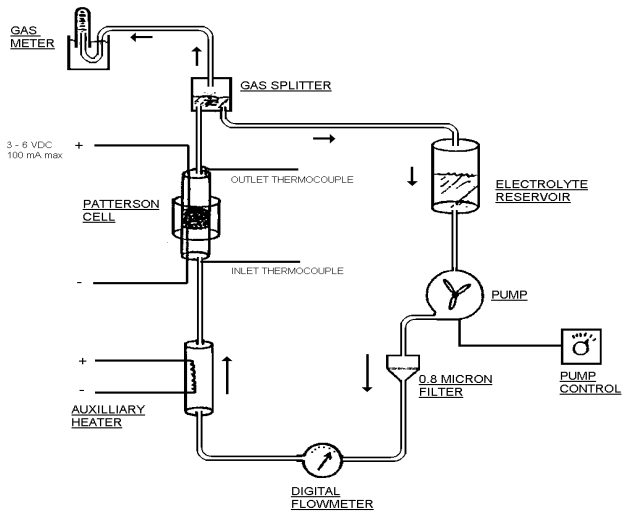

Fig. 1 b. Schematic of flow system.

state, was about an hour for the present Ni run. Thus this loading time was negligible compared to the two-week run time. A quantitative measurement of the loading was not attempted, although there is strong evidence presented by others that loadings in excess of 0.85 atoms of hydrogen or deuterium (H/D) per atom Pd are required in conventional solid Pd electrodes to produce heat (Crouch-Baker et al. [3]). After an equilibrium was achieved, the cell inlet temperature was raised slowly (over several hours) to the desired operating temperature of 60-70° C.

Further details about construction and operation of this type of cell is given in Patterson [24], Cravens [2], and Nix et al. [21].

NICKEL-FILM RUN

The run lasted for 310 hours and employed an entering electrolyte temperature of approximately 60° C. Termination of the run was made prior to any noticeable deterioration of thermal performance. A temperature rise across the cell of less than 0.5° C was obtained throughout the run, representing an output of 0.5 ± 0.4 watts. Calibration corrections due to heat losses and flow-pattern variations prevented a more accurate measurement, but the output always indicated a positive excess heat.

The cell employed for the run used all plastic fittings with the exception of the pressure and flow meters and the pump. (To further decrease possible impurity sources, a loop with all plastic components except for the electrodes was developed for subsequent runs. As noted later, this modification did not cause a noticeable change in film products.) Titanium electrodes were used. A filter fitted with 0.8-μm pore size filter paper was inserted in the loop to collect any fine particles entering the electrolyte, either from film surfaces or from other parts of the system.

Characteristics of the 650-Å Ni film microspheres used in this run (#8) are summarized in Table 1. A 650Å-thick Ni film was laid down by sputtering the Ni on to a 1-mm plastic core. The thickness of the layer was determined by weighing a calibration sample coated under the same conditions as the microspheres in the sputtering unit. Some coating variations, estimated to be ±30%, can occur among the 1000 microspheres used in the cell, however. Measurements with an Auger electron probe on select microspheres confirmed the film thickness to be reasonably uniform (±20%).

Table 1 Data for nickel coated microspheres

Layer	Diameter (cm)	Volume (cc)	Mass of layer (g)	# of atoms
PS	0.106	6.22×10^{-4}	6.09×10^{-4}	
Ni(605A)	0.106	2.29×10^{-7}	2.04×10^{-6}	2.09×10^{16}

Total Mass of a microsphere 6.11×10^{-4} g.
Total Mass of metal on a microsphere 2.04×10^{-6}
Total Atoms of metal 2.09×10^{16}

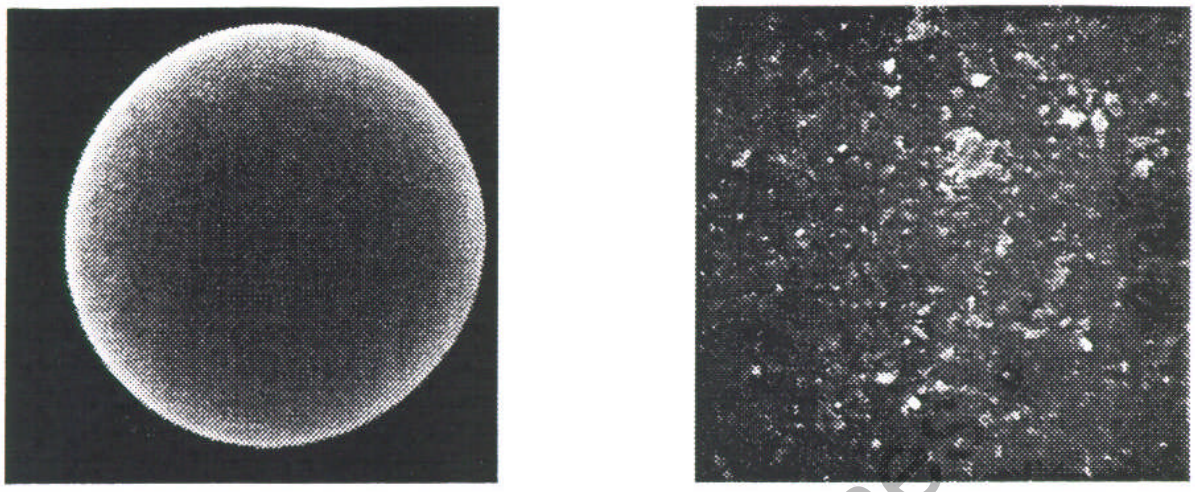

Fig. 2a. SEM photographs of the microsphere before a run (80X magnification on left & 1000X magnification on right).

The mass of the metallic film on these microspheres was less than 1% of the total microsphere mass (see Table 1), giving a most unique electrode configuration for the electrolytic cell. Photographs of the outer surface of the microspheres, using a scanning electron microscope (SEM), confirmed that a very smooth surface was achieved with the sputtering process (Fig. 2a), while a high magnification photo shows a small-scale, rough structure uniformly distributed over the surface. Some erosion of small particles from the surface occurs during operation, however, as detected by placing a filter with 0.8-μm filter paper in the flow loop. Concurrently, various fragile looking bead-like and fiber-like structures are typically visible on the film surface after electrolysis, e.g., see Fig. 2b.

REACTION PRODUCT ANALYSIS METHODS

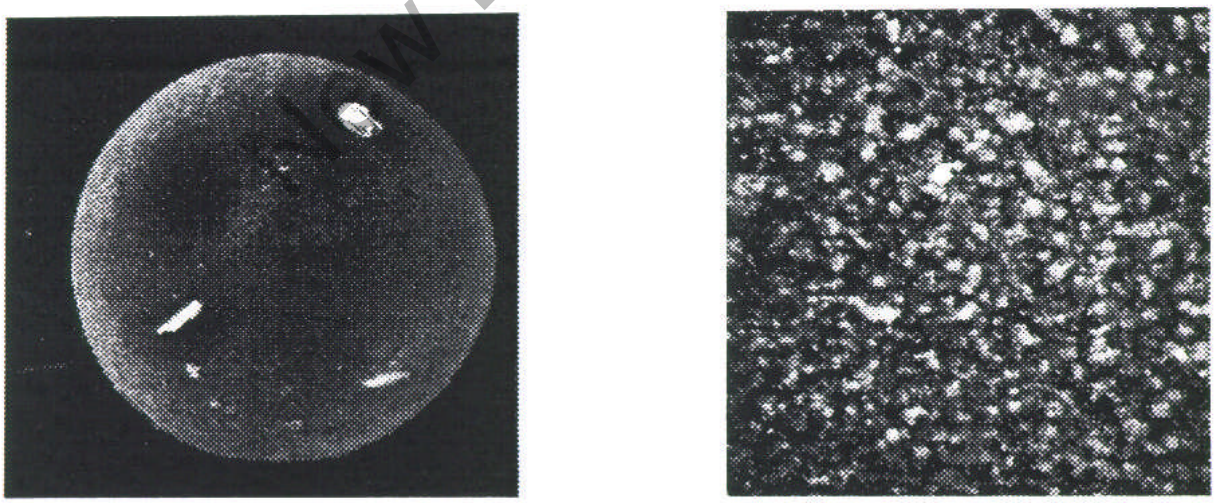

Fig. 2 b. SEM photographs of the microsphere after a run (80X on left & 1000X on right).

SIMS, EDX, AES and NAA methods were employed to analyze the microspheres before and after the run. Sampling was done by disassembling the cell after a run and removing microspheres from the top (cathode end) layer of the packed bed. (The 1000 microspheres in the bed result in roughly 3-5 layers total). These microspheres were selected for reasons of accessibility and the fact that the higher electric field in that region is expected to make this layer most reactive.

This limited selection procedure raises key issues about the reactivity in other layers. Thus, an uncertainty arises when it is desired to extrapolate the results to predict total cell characteristics (element yields or cell power). To study these effects in more detail, a new sampling technique employing a small plastic tube that is plunged into the bed to extract a "core sample" of microspheres has now been developed.

The SIMS analysis employed a Cameca IMS 5F unit operating with 8-keV oxygen primary beam in the positive ion mode (Wilson et al.[27]). Scans of key isotopes were made using single microspheres in a low-resolution (2,000 mass resolution) mode at several depths of interest (typically near the surface and interfaces) (see Fig. 3a). High-resolution (40,000 mass resolution) scans were then done to resolve any interferences involving important isotopes (e.g., see Cu-63 and Ag-107 in Fig. 3b). Although the SIMS gives the relative amounts of isotopes for a given element accurately, the variation of isotopes with depth and the lack of reference samples for calibration of the SIMS sensitivity made it difficult to determine absolute concentrations of isotopes with this technique alone. Thus NAA was used to determine total concentrations of Al, Cu, Mg, Cr, Fe, Zn, V, and Ag (subsequently termed "NAA elements") in the microspheres. This data was, in turn, used as a calibration for the SIMS sensitivity to find concentrations of the other "non-NAA" elements, as described next.

SIMS scan of a fresh microsphere (See all figures at end of paper.)
Fig. 3a. Typical low resolution SIMS scan (before the run).
Fig. 3a. Typical low resolution SIMS scan after the run (average of microspheres in 3 layers in the cell).
Fig. 3b. High Resolution SIMS scan for Cu(63) after the run.
Fig. 3b. High Resolution SIMS scan for Ag(107) after the run.

Interpretation of the SIMS count data of Fig. 3 requires a knowledge of sensitivities (RSF values) for sputtering of each isotope out of the host matrix by the SIMS's primary beam (Wilson et al. [27])

For accurate analysis, the RSF should be determined by implanting a known quantity of the isotope of interest in a sample of the host matrix and measuring the RSF in the SIMS under the actual conditions employed. Since such a calibration is not available for thin film Ni, an alternate technique was employed. Theoretically (Wilson et al. [27]), the RSF is an exponential function of the ionization potential (IP) for non-gaseous isotopes in a fixed host matrix. This functional relation was employed, but a RSF-IP slope from Ni matrix studies by Wilson and Stevie [28][29], and Wilson [28] was assumed and fit through data for the nine NAA elements to obtain a RSF value for the remaining SIMS values. One refinement found necessary was to separate elements into two groups, one having concentrations >0.1% and one <0.1%, each group having a different RSF functional fit. (SIMS intensities tend to saturate at high concentrations.) With this technique, an uncertainty factor of 2 is estimated for the absolute values for non-NAA element percentages. (Note: due to changes in the RSF correlation employed, results presented here differ somewhat for those in an earlier draft of this paper, cf. G. Miley and J. Patterson [16]).

NAA was carried out at the University of Illinois (UI) TRIGA research reactor (Landsberger [9]). Samples consisted of 10 microspheres. Techniques for short-lived NAA (Parry [23]) were initially performed to determine the presence of Ag, Cu, Al, and V in the electrodes. (Subsequently, analysis of Fe, Cr and Zn was done in a similar fashion.) Epithermal NAA was used for Ag in conjunction with the $^{109}Ag(n, \gamma)^{110}Ag^{m}$ reaction using the 657.1-keV gamma ray. A 10-sec irradiation time at a flux of 2.1×10^{11} n/cm^2·sec, with a 20-sec decay time and a 75-sec counting time was used, along with a pneumatic transfer facility. Typical detection limits for Ag were of the order of 2 ppm, with a precision of ±10 to 15%. A typical gamma spectrum for the Ag analysis is shown in Fig 4a.

Fig. 4a. Typical NAA gamma spectrum for Ag.
Fig. 4b. NAA gamma spectrum for Cu.

Thermal NAA was also used for Cu, Al, and V in conjunction with $^{65}Cu(n,\gamma)\,^{66}Cu$, $^{27}Al(n,\gamma)\,^{28}Al$, and $^{51}V(n,\gamma)\,^{52}V$, using the 1039.1-keV, 1778.9-keV, and the 1434.2-keV decay gamma rays, respectively. A representative gamma spectrum for Cu-66 is shown in Fig. 4b. Typically, a 2-min irradiation time with a flux of $4x10^{11}$ $n/cm^2 \cdot sec$, followed by a 2-3-min decay time and a 5-min counting time was used with the same pneumatic transfer facility. Detection limits were several ppm for Cu and less than 1 ppm for V and Al, with a precision of several percent for these elements. Calibration used certified liquid standards from the National Institute of Standards and Technology. Ores containing known quantities of these elements were analyzed for quality control. All such NAA results agreed within the error limits of the reference materials.

As a supplement to SIMS analysis, NAA was also employed to study key isotope ratios for comparison to natural abundance. Cu and Ag are of particular interest in the present work. Then, for example, an NAA measurement of the Cu63/65 ratio was carried out. Cu-63 was determined using the $^{63}Cu(n,\gamma)\,^{64}Cu$ reaction with the resulting 511-keV gamma ray to determine Cu-63. Cu-65 was determined using the $^{65}Cu(n,\gamma)\,^{66}Cu$ reaction using the 1039-keV gamma ray (see Fig. 4b).

The EDX analysis used a Field Emission Electron Microscope (Hitachi S800) operating in the energy dispersion analysis mode with the electron energy set at 20 kV to detect elements with atomic concentrations above about 1%. LINK software was utilized to derive the elemental concentrations from the energy spectrum. Due to the unique geometry with the curved film-plastic interface, the measurement accuracy was limited to 10%.

AES was used in a sputtering mode to perform semi-quantitative depth profiling for the major element species above 1 atom %. Two instruments were employed, PHI models 660 and 595, providing a resolution of approximately 25 nm. Depth profiles were also run with the SIMS, but the higher sputtering rates for SIMS greatly limited the spatial resolution in the thin film.

RESULTS

ELEMENT AND ISOTOPE CONCENTRATIONS

Results from NAA and EDX analysis of high concentration elements (Mg, Al, Si, Ag, Cr, Fe, Zn, and Cu) in the Ni run are summarized and compared in Table 2. (Two NAA runs on the microspheres yielded values within 10% of those shown for NAA in the table). The variation in the concentrations observed is attributed to the fact that each analysis used a different sampling of microspheres taken from various locations in the packed bed at the end of the run. Some differences are expected from microsphere to microsphere due to variations in location and coating. Further, the NAA results provide total concentrations for a sample of 10 microspheres, while EDX examined only a small volume of an individual microsphere. Still, the important point is that these independent measurements confirm that following a run, over 40 atom % of the film consists of these product elements, the remainder being the host Ni plus trace elements.

Table 2. Comparison of NAA and EDX analyses for several microspheres

ANALYSIS COMPARISON (Atomic %) *

TYPE	NAA	EDX	EDX
Sample #	N3.3	N3.3	N3.3
Mg	NA	5.6	5.0
Al	0.51	2.3	2.2
Si	NA	7.3	6.1
S	NA	1.1	NL
Ag	6.61	17.0	30.7
Cr	5.94	6.9	6.5
Fe	14.53	17.2	10.3
Ni**	62.31	32.3	29.0
Cu	7.96	10.3	10.2
V	0.01	NL	NL
Co	0.10	NL	NL
Zn	2.04	NL	NL
Total	100.0	100.0	100.0

** microspheres taken from same location in the packed bed.*
*** Ni % (from NAA) adjusted for a total of 100%*
NA: Not included in analysis
NL: Percentage below detection limit

To evaluate the other major **non-NAA** elements present and to obtain isotopic concentrations, SIMS and NAA data have been combined in Table 3. **NAA elements** are listed in bold. (Light elements, still under study, and other isotopes not observed are omitted from Table 3.) This table shows the yield, i.e., the difference between the final and initial weight for each isotope (fourth column). NAA only measured the elemental (isotopic) concentrations; therefore the NAA values for a given element have been pro-rated between isotopes according to the SIMS isotopic analysis. Corresponding values for the number of atoms of each isotope before ("fresh MS") and after ("reacted MS") a run follow in the fifth and sixth columns. Non-NAA elements used the SIMS data directly for both the element yield and the isotope values, based on the RSF interpretation discussed earlier.

Table 3. Yield Data from the Combined SIMS/NAA Analysis [see remaining figures at end of paper.]

Despite the uncertainties associated with the RSF correlation for non-NAA elements, the values shown in Table 3 should still provide a first estimate of ***non-NAA*** isotopes in the film. Note that the isotopic yields for **NAA elements** should be quite accurate, since the RSF values are essentially constant for isotopes of a given element, while the total concentrations of these elements come directly from the NAA measurement, avoiding RSF issues.

The isotopic atomic percents in the metal film are then calculated from the increased number of atoms for each element (column 7) and tabulated in the column labeled "SIMS". Comparison of this result with natural abundance values ("Natural a/o" in column 3) gives the "difference in a/o" shown in the final column. This data in Table 3 is used later to obtain figures for element production rates (Fig. 7 and Fig. 8), element yields (Fig. 9a and Fig. 9b), and isotope shifts (Fig. 11) vs. mass or Z. The systematics of the data will become clearer when these figures are discussed.

ELEMENT DEPTH PROFILES

Data from AES profile measurements on a typical microsphere are presented in Fig. 5 for the higher concentration elements. While the isotopes' profile behaviors are hard to interpret quantitatively, several observations can be made. Most profiles peak in the nickel volume or near the film-plastic interface, suggesting an internal source rather than diffusion in from the surface. For example, the key elements Ag and Fe peak near the Ni-plastic interface, (at ~ 650 Å corresponding to about 12 min. sputtering time). Cu peaks further out in the film. However the amplitude of the peaks is too small to draw definitive conclusions about diffusion vs. an internal source.

The product concentrations decrease into the plastic substrate. However, the decrease is gradual, indicating strong interdiffusion has occurred under run conditions. This interdiffusion of products can explain some differences between NAA and EDX values noted earlier in Table 2, since NAA, in contrast to EDX, measures total amounts of elements throughout both the film and the core of the microsphere. This distinction also applies to NAA vs. SIMS measurements.

Approximate Depth (Å)	0	100	700	2000
	Relative Atomic %			
C	20.00	-	-	61.23
Ag	2.68	9.94	11.77	3.07
Fe	7.72	10.02	10.45	5.12
Ni	9.99	12.30	22.28	12.56
Cu	4.17	7.64	7.61	5.38
Zn	11.12	10.48	9.22	-
Mg	10.78	13.75	-	-
Cr	-	-	3.66	4.99

Fig. 5. Tabulated atomic % vs. depth from AES scan.

NUCLEAR RADIATION EMISSION

In view of the evidence that products are formed at a significant rate (order of 10^{15} reactions/s-cm^3, cf. Table 5, discussed later) in an operating cell, measurable radiation emission would normally be expected, assuming normal nuclear reactions. However, so far attempts to measure nuclear radiation emission-neutrons, gammas, or x-rays-during cell operation have not detected any measurable quantities above background. A ^{3}He detector was employed for neutron measurements, and a cooled NaI crystal detector was used for gammas and x-rays. In one run, a 5-mm-thick Be window was placed over a small hole drilled into the side of the cell to allow measurement of softer x-rays (estimated lower limit of 20 kV), but after a four-hour run, none were detected. It is planned to repeat these measurements in a shielded area to reduce the background; however, if radiation emissions are escaping the cell, they are very low in intensity.

Another measurement used a liquid-scintillation detector to search for tritium in a sample of electrolyte immediately following a run. This measurement was repeated, and a sample was also sent out for independent analysis, but in no case was tritium detected. An experiment to measure the presence of tritium in the off gas, along with other possible products such as ^{4}He, is under consideration, but due to the very low concentrations involved, such measurements become very demanding.

Two attempts to measure beta or x-ray emission from the microspheres after a run were made by placing them on the face of a liquid N_2 cooled NaI crystal detector covered with a thin Be foil, but without positive results. Next, a set of microspheres was placed on medical X-ray film for a 3-day exposure – again negative results. Subsequently, a sample of microspheres run several months earlier were placed in a liquid scintillator and counted for three hours, using a Packard Tri-Carb 1500 dual-channel liquid-scintillation detector. No significant reading above background was obtained.

Recently, several sets of microspheres (run about 4 months earlier) were exposed to high-speed ASA 3000 film for a 4-day period with positive results as shown in Fig. 6 (Klema, 1996 [8]). Unfortunately, these experiments are not yet reproducible. A second positive exposure has been obtained, but three additional attempts failed. The technique is under study, and if verified, will demonstrate emission of low-energy beta rays or soft x-rays (estimated to be of the order of 20 keV for the geometry of Fig. 6).

Fig. 6. Nickel Microsphere Exposure on Kodak ASA 3000 Polaroid Film.

In summary, there is very preliminary evidence for soft x-ray (<20 keV) or beta emission from microspheres after operation. There is not an easily measurable emission of other high-energy radiation from the microspheres after operation or from the cell during operation. These facts must be considered when possible reaction mechanisms are sought to explain the present results. Much more study is needed, however, to fully define possible radiation emission for these cells.

MASS BALANCES AND IMPURITY ISSUES

The use of thin films introduces a problem in reaction product studies due to the small volume occupied by the film vs. the large volume of the electrolyte – about 100 cm^3 electrolyte vs. 3 x 10^{-4} cm^3 film for 1000 microspheres in the bed (cf. Table 1), a volume ratio of $\approx 10^5$:1. The corresponding mass ratio is roughly the same; consequently a low ppm impurity in the electrolyte could, if concentrated in the film, give a very high ppm there.

Note that some of the key elements are present in trace (but measurable) quantities in the applied thin film; e.g., recall Table 3. However, the initial values are typically a small fraction of the final, and they are always subtracted from the analysis of the increase in concentration of an element used to report yields and production

rates. Thus the key issue is whether there is another source of these isotopes in the cell or loop. Potential sources of impurities include the Li_2SO_4 itself, the cell glass, the insulating anode salt beads, the Ti (or Pt_{in} some cases) electrodes, and other loop components. Those components which were easily accessible plus the electrolyte and filter paper were analyzed by NAA since higher precision is required than is possible using manufacturer's specifications for impurities.

Masses for representative key elements (Ag, Al, Cu and V) based on NAA analyses of the microspheres, the electrolyte, and the filter paper are summarized in Table 4a. The key potential source of impurities in the microsphere film is the electrolyte. However, as seen from the table, the ratio of total mass of the four key elements in the electrolyte to that in the thin film was < 10% for Ag, Cu, and V, but was comparable for Al. Thus, at least for the first three elements, impurities in the electrolyte could not possibly account for present observations

Table 4a. Key element mass balances from NAA on microspheres, electrolyte and filter paper before and after a run. (see next page)

Impurities on the filter paper itself are also negligible. The total impurity masses in the electrodes are larger, but most of it is not "accessible." For example, while the Ti electrode was 100 μg Cu, if it is assumed as much as 1% of the Ti in the anode was dissolved and deposited in the Ni film, the Cu would be only 1 μg, or 0.1% of the increased Cu found there. Examination of anode surfaces after the runs indicates no observable erosion. Further, if large erosion occurred, more Ti would be expected on the microsphere surfaces than was found. Thus, the 1% erosion assumed here is, if anything, a gross overestimate. For these reasons, the Ti anode cannot account for the observed elements in the Ni film, and the ppm of other elements in the electrode rule it out as their source also. Analyses of the plastic components and other fittings leads to a similar conclusion for them. In no case is the upper limit for the amount of accessible material in any system component (singularly or taken together) enough to account for the key element concentrations found in the microsphere films, Al being a notable exception.

Balances for the many other elements found in the film have not been carried out (other than for subtraction of initial amounts found in the film by NAA or SIMS prior to a run). Thus, there remains a concern that some may be associated with trace impurities. Still, a number of the products found are not nominally anticipated to be present in materials used in the experiment. Thus, the likelihood that the entire array could have this origin seems unlikely.

Several additional checks on possible component contamination were run. In one, special microspheres with a conducting surface created by sulfonation were run in the cell with a voltage-current applied to simulate a Ni run. Subsequent NAA analysis of the microspheres (see Table 4b) and the filter paper showed that no build up of the important elements occurred on them. In this case, if impurities were present from a loop component, larger changes in the element concentration on the sulfonated beads than seen in Table 4b would be expected. (Changes there lie within the accuracy limits for NAA and microsphere-to-microsphere variation.) In another run, the cell was filled with glass microspheres and run at elevated (~60° C) temperature but without an applied voltage. Again no impurity build up was found.

Additional strong evidence was obtained in more recent work where runs are done in a special "clean" cell where all plastic parts are used in the loop except for the electrodes. The electrolyte is further purified by pre-test runs. Results from operation with this new cell are still being analyzed, but preliminary results confirm that the elements reported here are still formed despite the further reduction of possible impurities.

There is additional extremely strong evidence that the reaction products are not from external source contamination. First, many of the products observed show shifts from isotopic ratios in natural elements (seeFig. 11, discussed later), uncharacteristic of normal impurities. Second, in the other runs (not presented here) many

Table 4a.

Key element mass balances from NAA on microspheres, electrolyte and filter paper before and after a run

Microspheres

Element	ppm (fresh)	ppm (used)	Mass diff (g) / 1000MS
Ag	125.4	2594.9	1.51E-03
Al	11.2	50.2	2.38E-05
Cu	27.0	1840.9	1.11E-03
V	0.1	2.6	1.52E-06
Cr	2.9	1126.4	6.87E-04
Ni	1821.0	4420.5	1.59E-03
Fe	217.2	2956.6	1.67E-03
Zn	15.4	488.8	2.89E-04
Co	0.6	20.5	1.22E-05

used det. limit for ppm of Fe & Zn

Filter Paper

Element	ppm (fresh)	Mass in sample
Ag	0.0	8.79E-09
Al	0.9	7.07E-07
Cu	2.0	1.62E-06
V	0.0	7.79E-09

Filter Paper

S.No:	89.0
M(sample):	0.81

Electrolyte

Element	ppm (fresh)	Mass in system
Ag	0.03	3.00E-06
Al	2.2	2.20E-04
Cu	0.8	8.00E-05
V	0.01	9.00E-07

Electrolyte

S.No:	83.0
M(sample):	0.82
Initial Vol.(ml)	100.0
Times Filled	1.0
M(in system)	100.0

Electrode Material (Ti; two electrodes)

Element	ppm (fresh)	Mass in sample
Ag	1.3	1.15E-06
Al	84	7.46E-05
Cu	120	1.07E-04
V	215	1.91E-04

Ti electrode

S.No:	85.0
M(sample):	0.044
M(of electrode):	0.444
# of electrodes:	2.0
M(in system):	0.89

* all masses are expressed in grams
* M : abbreviation for Mass
* S. No. : abbreviation for Serial Number
* MS : abbreviation for Microsphere

Table 4b.

NAA result for sulfonated polystyrene microspheres

Element	ppm (before run)	ppm(after run)
Ag	0.7	2.9
Al	123.0	133.2
Cu	64.2	35.1
V	0.8	0.2

different elements are found, varying according to the material used for the thin film. If the source were elsewhere in the loop, the same elements would be expected, irrespective of the specific film material. Third, as discussed later, the yields of key elements appear to be consistent with independent results from different, but related experiments by Mizuno et al.[19], and Ohmori and Enyo [22]. Such a coincidence seems unlikely if impurities were involved due to the differences in experimental set-ups.

A noteworthy point related to mass balances is that noticeable quantities of materials were collected on the filter paper during the run, but this material is attributed to particles breaking off of the film surface under operating conditions. A SEM photograph of the debris on the filter paper after the nickel run is shown in Fig. 7. A thin solid layer of cake-like material is visible, with larger flakes on top plus small droplets, both of which appear to come from the bead surface (cf Fig. 2). Additional evidence that this material came from the film is based on runs where conducting plastic or glass microspheres were employed and material paper on the filter did not collect, confirming that this material does not originate from the electrode, cell walls or other loop components. NAA shows a composition similar to the film. Thus if elements contained in these materials were included in the analysis as belonging to the film, even larger yields would be reported.

Fig. 7. SEM photograph of debris on filter paper.

In summary, the finding that the masses of the key isotopes are large compared to possible sources of such isotopes from loop components, the negative results from simulation runs without Ni films, the observation of isotope shifts from natural abundance, and the observation that the isotopes vary with film material, combine to provide very strong evidence that the products reported are due to nuclear reactions. The next issue is to consider what reactions can account for these observations.

REACTION PRODUCT SYSTEMATICS

PRODUCTION RATES

Based on the yield data presented earlier, time-averaged element production rates are computed in Table 5 and plotted in Fig. 8a and Fig. 8b in terms of weight fraction of the metal film/s-cm^3 of film and atoms/s-cm^3 of film, respectively. These figures assume that the production rate was constant

Table 5 Production rate data.

Z	Element	Atomic Wt.	Yield (per microsphere) (frxn./s/cc)	(atom/s/cc)
14	Si	28.09	1.08E-01	2.25E+15
16	S	32.06	3.37E-02	7.04E+14
21	Sc	44.96	1.12E-04	2.34E+12
22	Ti	47.88	9.88E-03	2.06E+14
23	V	50.94	4.46E-04	9.31E+12
24	Cr	52.00	2.27E-01	4.75E+15
26	Fe	55.85	2.70E-01	5.64E+15
25	Mn	54.94	1.50E-01	3.13E+15
27	Co	58.93	2.96E-03	6.18E+13
29	Cu	63.55	2.78E-01	5.81E+15
30	Zn	65.39	6.15E-02	1.28E+15
31	Ga	69.72	2.26E-04	4.73E+12
32	Ge	72.59	1.75E-02	3.65E+14
34	Se	78.96	1.88E-01	3.92E+15
33	As	74.92	7.37E-02	1.54E+15
38	Sr	87.62	2.74E-05	5.72E+11
37	Rb	85.47	1.07E-06	2.24E+10
39	Y	88.91	4.28E-05	8.93E+11
40	Zr	91.22	9.25E-05	1.93E+12
42	Mo	95.94	4.29E-04	8.96E+12
41	Nb	92.91	9.89E-05	2.06E+12
46	Pd	106.42	1.26E-02	2.62E+14
48	Cd	112.41	2.12E-01	4.43E+15
47	Ag	107.87	1.69E-01	3.53E+15
50	Sn	118.71	5.77E-03	1.21E+14
49	In	114.82	4.78E-05	9.97E+11
52	Te	127.60	1.40E-02	2.93E+14
51	Sb	121.75	4.72E-03	9.85E+13
56	Ba	137.33	4.88E-04	1.02E+13
62	Sm	150.36	8.52E-05	1.78E+12
63	Eu	151.96	3.91E-05	8.16E+11
64	Gd	157.25	3.15E-04	6.57E+12
66	Dy	162.50	2.01E-05	4.20E+11
67	Ho	164.93	2.34E-05	4.89E+11
70	Yb	173.04	3.44E-05	7.19E+11
82	Pb	207.20	5.50E-03	1.15E+14

over the 310 hour run. There is some preliminary indication that the rate is higher at the start, and the time dependence, along with the effect of microsphere location, is now under study.
As seen from Fig. 8a, the large yield elements Cr, Fe, Se, Cu, Cd, and Ag have weight fraction (μg of element per μg metal film at start of run) production rates exceeding 0.1/s-cm^3. This corresponds to a rate of roughly 10^{-4} μg/sec for the full 1000-microsphere cell, or a run total of roughly 1 mg/element. In terms of atoms produced, the high yield elements have rates of ~10^{16}/s-cm^3, suggesting a nuclear reaction rate of corresponding magnitude.

Then assuming these five elements dominate and are created at 10^{16}/s-cm^3 each, operation at 0.5 watts for the 1000-microsphere cell corresponds to an average energy release of roughly 6 x 10^{-2} MeV/atom reacting Such an energy release is easily obtained by various exothermic nuclear reactions (Miley [13]) but as discussed later, due to the formation of heavy elements like Cu, Ag, and Cd, some endothermic reactions "absorb" energy. Thus the 0.5 W excess must be viewed as a "net" energy release from these various reactions.

The corresponding total increase in element masses, or in element atoms, are presented in Fig. 9a and Fig 9b, respectively. Consistent with the production rate graphs, these figures show total yields per microsphere approaching 0.1-0.2 μg per high yield element, or 3-6 atomic % in the metallic film.

It is interesting to compare these results to those reported by Mizuno et al. [18], who ran a high-current-density Pd electrode in a cell at high pressure and temperature with a heavy water Li_2CO_3 electrolyte. They report a rich variety of reaction products at 1-mm depth, concentrated in groups with atomic numbers 6 , 20-30, 46-54, and 72-82. Earlier, Bockris and Minevski [0] had reported a similar array of elements beneath the surface of a Pd electrode, separated from surface impurities. While isotope shift studies were not undertaken, they argued that these elements were not impurities based on diffusion considerations. While a one-per-one comparison is not possible since the present study used Ni rather than Pd, this distinct grouping of products is consistent with the present results where major products group between Z = 12-14, 20-30, and 46-56. The resemblance is seen from Fig. 10, where Mizuno et al.'s (and also Bockris and Minevski's) results are superimposed on the present data. Since neither Mizuno et al. nor Bockris and Minevski reported absolute yield values or rates, for comparison, their results have arbitrarily been normalized to the present Cu production rate. With this normalization, a number of the production rates for other high yield products agree reasonably well with Mizuno et al's results, e.g., note from Fig. 10 that Si, Cr, Fe, and Cd lie close together. Agreement with the Zn and Ag yields from Bockris and Minevski's experiment is good, but their other high yield products (Mg, Si, Ca, Fe, Pt) have somewhat higher production rates than found in the present Ni microspheres. A larger variation in lower yield elements is observed among these three experiments where various elements are found in one experiment and not the others. Two noticeable differences are the high yield of gases (Xe and O) and the yields at high Z72-82 group, including Os, Au, Hg found by Mizuno et al., and Pt found by Bockris and Minevski. Differences in gas yields might be anticipated. Gases are expected to diffuse out of the thin films used in present work, hence would not be found in SIMS results. The reduction of other products in the 72-82 group in present experiments is probably associated with the use of the lower Z Ni host material (vs. Pd). In conclusion, the resemblance of certain key features of the present results and those of Mizuno et al., and also Bockris and Minevski, is striking. In niew of the major differences in cell construction, this resemblance adds credence to the already strong arguments by all three experimental groups that the observed elements are not impurities.

Fig. 10. Comparison of present production rate data with Mizuno et al. and Bockris and Minevski.

The large production rate of Fe found here also has a resemblance to the observation by Ohmori and Enyo [22] that notable amounts of Fe was formed in electrolytic cells with Au and Pd electrodes and various light water electrolytes. They report Fe yields of ~10^{16} atom/cm^2 (17μg and 38μg maximum from Au and Pd electrodes, respectively). The present Fe production rate of 5.4 x 10^{15} atoms/s-cm^3 (cf Fig. 8b or Fig. 10) corresponds to 5.9 x 10^{21} Fe atoms/cm^3-film. For the 650-Å film thickness, this is equivalent to about 3.8 x 10^{16} Fe atoms/cm^2, in reasonable agreement with Ohmori and Enyo's measurements. The yield of Fe in present work from Fig. 9a

is ~0.22μg/microsphere, or ~0.2 mg total for the 1000 microsphere cell -- about 10 times the Ohmori-Enyo yield. A major factor in the higher yield is probably the larger surface area (~32 cm^2) of the microspheres vs. the 5-cm^2 plates used by Ohmori-Enyo. Other factors, such as input power, electrolyte, etc. must also affect the results, but attempts to optimize cell conditions in these varied experiments seem to have resulted in amazingly similar Fe production rates.

ISOTOPE SHIFTS FROM NATURAL ABUNDANCE

Differences between the isotopic percentage concentrations observed with the SIMS vs. those for natural abundance for the reaction product elements, listed earlier in Table 3, are summarized in Fig. 11. The accuracy of these measurements is estimated to be of order of ±3% in the difference when high resolution is employed. High resolution was used to eliminate possible line overlap in all important cases, but with the large number of elements found, this was not possible for all of the lower yield isotopes. Thus, those results must be viewed as less certain. Of the higher concentration elements, Fe and Zn, show significant deviations. Cr and Ag are in the ±3-5% range, while Cu is in the ±1% range. Many low-concentration elements show quite large differences e.g., Ti-50, +77.7%; Ge-72, +21%; Se-82, +32%; Zr-96, +97%; etc. There are no obvious patterns, however.

Fig. 11. Isotope shifts (percent SIMS - percent natural abundance) vs. Mass Number, A.

To further study the deviation from natural abundance for the vital isotopes of Cu (Cu-63 and Cu-65) and Ag (Ag-107 and Ag-109) special NAA isotope measurements (described earlier) are underway. First results for the present Ni run, based on a sample of 10 microspheres, indicates a deviation from natural % abundance of +3.6 ± 1.6% for Cu-63 and -8.1 ± 3.6% for Cu-65. (Since the two results are from different lines, unlike SIMS, slightly different values can occur in the + and - values for pairs.) These results are to be compared to a deviation of +0.8% for Cu-63 and -0.8% for Cu-65 from the SIMS data. The reason for larger percent differences with NAA than SIMS is not clear. A possible explanation is that as stressed earlier, the SIMS results are localized on a spot on a single bead film whereas the NAA value represents the ratio of total amounts of each isotope contained in films on the 10 microsphere sample. These issues are now under study employing multiple measurements with a sample matrix of microspheres.

The trend in the Cu shifts found here is similar, but smaller, than reported by Mizuno et al. [19] who cite Cu-63, +25% and Cu-65, -25%. Shifts for Fe have been reported by Mizuno et al. and also by Ohmori and Enyo [22], and are compared to present results in Table 6. While differences are observed, two isotopes, 56 and 57, do show the same trend for all cases.

Table 6 Isotope shifts reported for Fe in various systems.

		Difference from a/o, in percentage			
		Present	Ohmori/Enyo		Mizuno et al
		Ni*	Au	Pd	Pd
	Nat a/o				
Fe-54	5.8	-0.1	+0.7	+2.0	(a)
56	91.7	-4.8	-14.2	-6.3	-21
57	2.2	+5.2	+12.3	+4.0	+20
58	0.3	-0.3	+1.2	+0.3	(a)

*Electrode Material
(a) Not Reported

While a more detailed comparison of the various shifts is not possible due to material differences, the observation of a large number of isotope shifts in Fig. 11 is consistent with the large number of deviations reported by Mizuno et al. [19] They used this observation to argue that the elements observed were due to nuclear reactions, rather

than impurities. The possibility exists for some isotope separation due to diffusion in the host metal, but that effect seems unlikely to account for the varied changes observed. In conclusion, Mizuno et al's isotope shift argument against impurity sources applies to the present results also, and, combined with the large product yields compared to possible impurity sources, strongly supports the nuclear reaction hypothesis.

REACTION MECHANISM CONSIDERATIONS

A nuclear explanation for the products observed here requires an entirely new theory for chemically assisted reactions in solids. Here it is possible only to point out some features that should be considered in such a theory.

As several workers have stressed (Miley et al. [11], Preparata [26], Hagelstein [4]), any theory for reactions in solids must explain: 1) how the reacting ions overcome the Coulombic barrier, and 2) what reactions take place after the ions interact. In the present case, the SEL theory cited earlier offers a possible explanation for overcoming the Coulombic barrier between ions in a thin-film electrode. While only a single film was used in the Ni run, a Fermi level difference can develop at the plastic/film interface or at any oxidized region on the outer surface. More work, is needed to obtain definitive evidence for the validity of this theory, however. And even if SEL theory is accepted, the key issue of what reactions occur after barrier penetration remains open.

In view of the large yields obtained, the reactants must involve some of the key species present, namely: Li, S, or O from the electrolyte; C and H from the plastic microsphere core; Ni from the thin films (cathode); and protons (p) from the light water. The isotope yield profiles do not indicate that elements from the electrolyte participated in the transmutations. Further, unpublished results (J. Patterson, 1996b [25]), indicate that operation with a Na-based electrolyte (vs. Li) results in similar heating rates. Carbon from the plastic can not be ruled out, but is viewed as an unlikely participant. For these reasons, the following assumes that the main reactions involve p-Ni interactions, with protons possibly coming from the plastic core as well as the electrolyte.

The concept that excess heat from electrolytic cells originates from reactions involving the electrode material, e.g. Pd electrode, is not new. Indeed, Ragheb and Miley [11], originally proposed that in a heavy water cell, Oppenheimer-Phillips-type neutron-stripping reactions between the D and Pd might explain early observations. Later, Miley (Appendix B in Hoffman [13]) summarized the status of such theories, and ironically introduced a table of possible p-Pd reactions (including examples of fission-type reactions). The present Ni results add a new dimension to these thoughts, however.

The present data provides information on a number of characteristics that any successful model must explain. Most importantly, the model must predict the large yields of the high-concentration elements, without introducing added products not observed. This fact alone rules out many possibilities, e.g., a simple p-Ni reaction followed by a succession of p reactions with products, plus fission of some elements (cf the multi-D Pd chain proposed by Mizuno et al. [19] to explain their Pd-heavy water results) fails this test.

In this respect, one aspect of present data noted earlier, is that gaseous products can diffuse out of the thin films. Thus, theoretical models with gaseous products, e.g., He, Xe, and Kr, should not be ruled out based on present data.

Other key features observed in Fig. 8 and Fig. 9 that must be accounted for by any theory include the "gaps" between high yield products and the high Ag and Cd yields. Ag (and Cd) production is particularly challenging, since Ag occurs in large quantities but is not favored energetically. Ag's position, well to the lower binding energy side of Ni, infers an endothermic reaction (negative Q-value), which in turn suggests energy transfer to the reactants must occur to drive the reaction. (This is analogous to driving negative Q-value reactions by colliding high-energy reactants using accelerated beams. As defined here, Q values are the energy released due to the mass difference between reactants and products, assuming that the reactants enter with zero kinetic or

excitation energy.) Consequently, the model must contain a mechanism for energy storage/transfer to reactions involved in high Z element production.

A postulated reaction model, RIFEX (Reaction in a Film-Excited CompleX), is under development to satisfy these key characteristics. A major feature of RIFEX is that protons (p) interacting with the host Ni and neighboring isotopes produces a relatively long lived atom-p complex with excitation energies of orders of several MeV. This allows production of elements such as Ag with −Q-value reactions. Other products are produced by negative Q-value reactions via fission of compound nuclei. This model will be presented in detail in a future publication.

CONCLUSIONS

The results presented here defy conventional views in many ways. First, chemically-assisted nuclear reactions are not widely accepted by the scientific community. The present results not only confront that disbelief, but add a new dimension to the issue by reporting copious light and heavy element reaction products that seem to imply multi-body reactions due to the formation of heavier elements such as Cu and Ag from Ni. Further, a reaction which does not emit intense high-energy gammas is required by the experimental results. All of these features are difficult to comprehend and at first glance seem to point to impurities. However, as stressed, an extensive effort to find an impurity source has not uncovered one. Also, there is other strong evidence (such as isotope shifts, the different products occurring when the coating material is changed, and the similarity in yield trends with results from other workers), which supports the conclusion that the elements observed are reaction products.

Fortunately, cell experiments of this type are relatively straightforward and inexpensive. Thus far, reaction products, such as reported here, have been detected by the authors in all dozen experiments of this type performed, using a variety of metallic films. In this sense, the phenomenon seems highly reproducible. The use of thin films as developed here offers a way to simplify the analysis since a large fraction of the film contains the new elements and their localization in the film allows a qualitative determination. Hopefully, open-minded scientists will attempt to replicate the experiments to convince themselves. If verified, the thin-film approach to chemically assisted nuclear reactions opens the way to a whole new field of science.

[For another explanation of overcoming the Coulomb barrier, see Shoulders & Shoulders, and Fox, Jin, & Bass papers in this issue. -Ed.]

REFERENCES

1a. J.O'M. Bockris and Z. Minevski, "Two Zones of Impurities Observed after Prolonged Electrolysis on Palladium," *Infinite Energy*, vol 1, no 5 & 6 (1996), pp 67-69.
1b. Bockris, J.O'M and G.H. Lin (organizers) (1996), Proceedings of the 1996 Low Energy Nuclear Reactions Conference, *J. New Energy*, vol 1, no 3.
2. Dennis Cravens (1995), "Flowing Electrolyte Calorimetry," Proc. 5th Intern. Conf. on Cold Fusion, Valbonne, France, IMRA Europe, pp 79-86.
3. S. Crouch-Baker, M.C.H. McKubre, F.L. Tanzella (1995), "Some Thermodynamic Properties of the H(D)-Pd System," Proc. 5th Intern. Conf. on Cold Fusion, Valbonne, France, IMRA Europe, pp 431-440.
4. Peter Hagelstein (1995), "Update on Neutron Transfer Reactions," Proc. 5th Intern. Conf. on Cold Fusion, Valbonne, France, IMRA Europe, pp 327-337.
5. H. Hora, J.C. Kelly, J.U. Patel, M.A. Prelas, G.H. Miley, and J.W. Tompkins (1993), "Screening in Cold Fusion Derived from D-D Reactions," *Physics Letters A*, vol 175, pp 138-143.
6. A.B. Karabut, Ya.R. Kucherov, and I.B. Savvatimova (1991), "The Investigation of Deuterium Nuclei Fusion at Glow Discharge Cathode," *Fusion Technol*., vol 20, pg 924.
7. A.B Karabut, Ya.R. Kucherov, and l.B. Savvatimova (1992), "Nuclear Product Ratio for Glow Discharge in Deuterium," *Physics Letters A*, vol 170, pp 265.
8. E. Klema (1996), Tufts University, Medford, MA. Private communication.

9. Sheldon Landsberger (1996), Dept. of Nuc. Eng., U. of Illinois, private communication.
10. M.H. Miles, and B.F. Bush (1994), "Heat and Helium Measurements in Deuterated Palladium," *Trans. Fusion Technol.*, vol 26, no 4T, Part 2, pp 157-159.
11. George H. Miley, Magdi Ragheb, and Heinrich Hora (1989), "Comments about Nuclear Reaction Products from Cold Fusion," NSF/EPRI Workshop, Washington D.C., 16-18 October 1989.
12. G.H. Miley, J.U. Patel, J. Javedani, H. Hora, J.C. Kelly, and J. Tompkins (1993), "Multilayer Thin Film Electrodes for Cold Fusion," Proc. 3rd Int. Conf. Cold Fusion (Frontiers in Science Series no. 4), ed. H. Ikegami, Universal Academy Press, pp 659-663.
13. G.H. Miley, (1995); in Hoffman, Nate (1995), A Dialogue on Chemically Induced Nuclear Effects: A Guide for the Perplexed about Cold Fusion, La Grange Park, IL, The American Nuclear Society, Appendix C, pp 146-154.
14. G.H. Miley, H. Hora, E.G., Batyrbekov, R.L. Zich (1994), "Electrolytic Cell with Multilayer Thin-Film Electrodes," *Trans. Fusion Technol*., vol 26, no 4T, Part 2, pp 313-320.
15. G.H. Miley, J.A. Patterson (1996), "Experimental Observation of Massive Transmutations Occurring in Multi-Layer Thin-Film Microspheres After Electrolysis," Abstracts, *Sixth International Conference on Cold Fusion*, Hokkaido, Japan.
16. G.H. Miley, and J.A. Patterson (1996), "Massive Nuclear Transmutations in Thin-Film Coatings on Microspheres Undergoing Electrolysis, Part 1--Nickel Films," Workshop, Clean Energy Technologies, Inc., Dallas TX, July 1996.
17. G.H. Miley, and J.A. Patterson (1996), "Design Considerations for Multilayer Thin-Film Patterson-Type Microspheres," Abstracts, *Sixth International Conference on Cold Fusion*, Hokkaido, Japan.
18. G.H. Miley, G. Name, M.J. Williams, J.A. Patterson, J. Nix, D. Cravens, H. Hora (1996), "Multilayer Thin-Film Microspheres after Electrolysis," Sixth International Conference on Cold Fusion, Hokkaido, Japan.
19. T. Mizuno, T. Ohmori, and M. Enyo (1996), "Changes of Isotope Distribution Deposited on Palladium Induced by Electrochemical Reaction," Preprint. [See also Mizuno et al. this issue. -Ed.]
20. Ira Myers, Gustave C. Frolick, and Richard S. Baldwin (1996), "Replication of the Apparent Excess Heat Effect in a Light Water–Potassium Carbonate--Nickel Electrolytic Cell," NASA Tech Memo 107167, NASA Lewis Research Center, Cleveland, Ohio.
21. John Nix (1996), "Revised Protocol for Patterson+ Cell Assembly and Operation," Confidential Memorandum, Clean Energy Technologies, Inc., 3 May 1996.
22. T. Ohmori, and M. Enyo (1996), "Iron Formation in Gold and Palladium Cathodes," *J. New Energy*, vol 1, no 1, pp 15-22.
23. Susan J. Parry (1991), "Activation Spectrometry in Chemical Analysis," in Chemical Analysis, ed. J.D. Winefordner, vol19, John Wiley and Sons, New York.
24. James A. Patterson (1996), "System for Electrolysis," U.S. Patent #5,494,559, 27 February 1996.
25. James A. Patterson (1996), Clean Energy Technologies, Inc., private communication.
26. G. Preparata (1991), "Cold Fusion: What Do the Laws of Nature Allow and Forbid?," The Science of Cold Fusion, Conf. Proc. 33, eds. T. Bressani, E. Del Giudice, and G. Preparata, Bologna, Societa Italiana di Fisica, pp 419-443.
27. R.G. Wilson, F.A. Stevie, C.W. Magee (1989), Secondary Ion Mass Spectrometry: A Practical Handbook for Depth Profiling and Bulk Impurity Analysis, New York, John Wiley & Sons. Wilson, R.G., 1996, Hughes Research Laboratories, private communication.
28. R.G. Wilson, F.A. Stevie (1996), "Secondary Ion Mass Spectrometry Depth Profiling and Relative Sensitivity Factors for Elements from Hydrogen to Uranium Implanted in Metal Matrices (Be, Al, Ti, Ni, Cu, W and Au)," private communication.
29. R.G. Wilson, F.A. Stevie (1991), "Secondary Ion Mass Spectrometry Depth Profiling and Relative Sensitivity Factors/Relative Ion Yields and Systematics for Elements from Hydrogen to Uranium Implanted in Metal Matrices (Be, Al, r, Ni, Cu, W and Au)," Proceedings of the Eighth International Conference on Secondary Ion Mass Spectrometry, John Wiley & Sons.

ACKNOWLEDGMENTS

This work was supported by a grant from CETI. The authors wish to acknowledge essential contributions to this effort by a number of individuals. G. Narne carried out experiments at the UI and assisted in both SIMS and NAA measurements. M. Williams (UI) was responsible for microsphere coating and for cell mechanics, and he coordinated microsphere analysis. J. Baker and staff at the Center for Microanalysis of Materials, UI, supervised the SIMS analysis and consulted on its interpretation. S. Landsberger (UI) carried out the NAA analysis and provided important insight into its interpretation. D. Cravens (CETI) was instrumental in the cell design, in

helping with numerous problems that arose during operation. J. Reding (CETI) helped coordinate the UI and CETI efforts and has provided most valuable encouragement and enthusiasm. R. Twardock (UI), carried out independent radiation measurements on the microspheres. E. Klema (Tufts U) carried out film exposures on the microspheres and provided valuable insights. H. Hora (UNSW) consulted on SEL and other theoretical aspects. Valuable comments on an earlier draft, by M. McKubre (SRI) and P. Hagelstein (MIT) are also gratefully acknowledged.

FIGURES

FIGURES

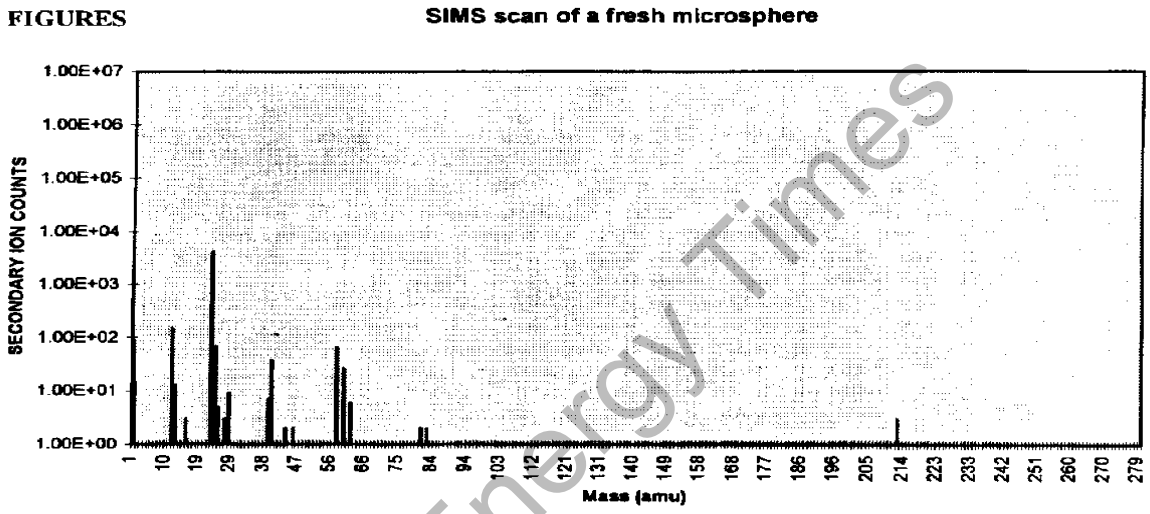

Fig. 3a. Typical low resolution SIMS scan (before the run).

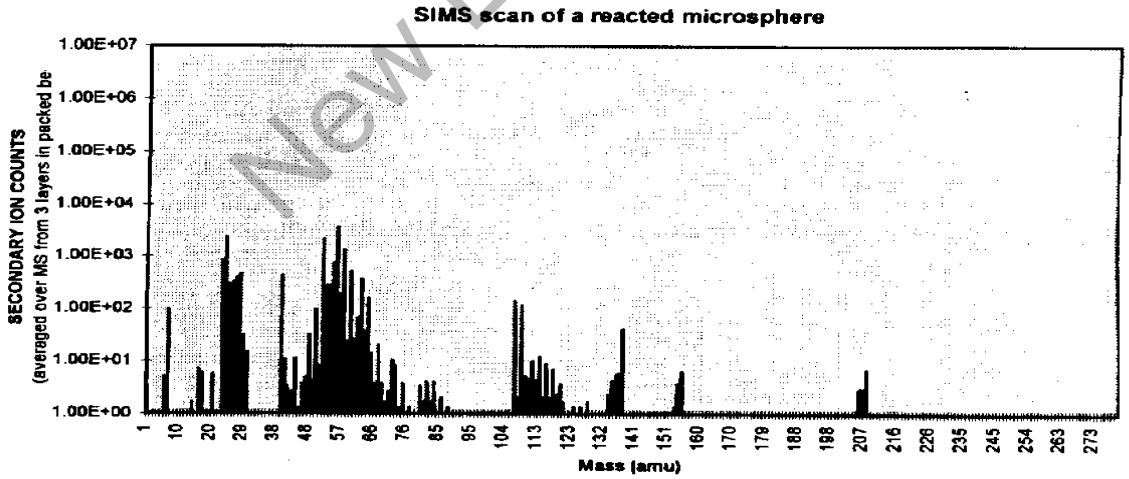

Fig. 3a. Typical low resolution SIMS scan after the run (average of microspheres in 3 layers in the cell).

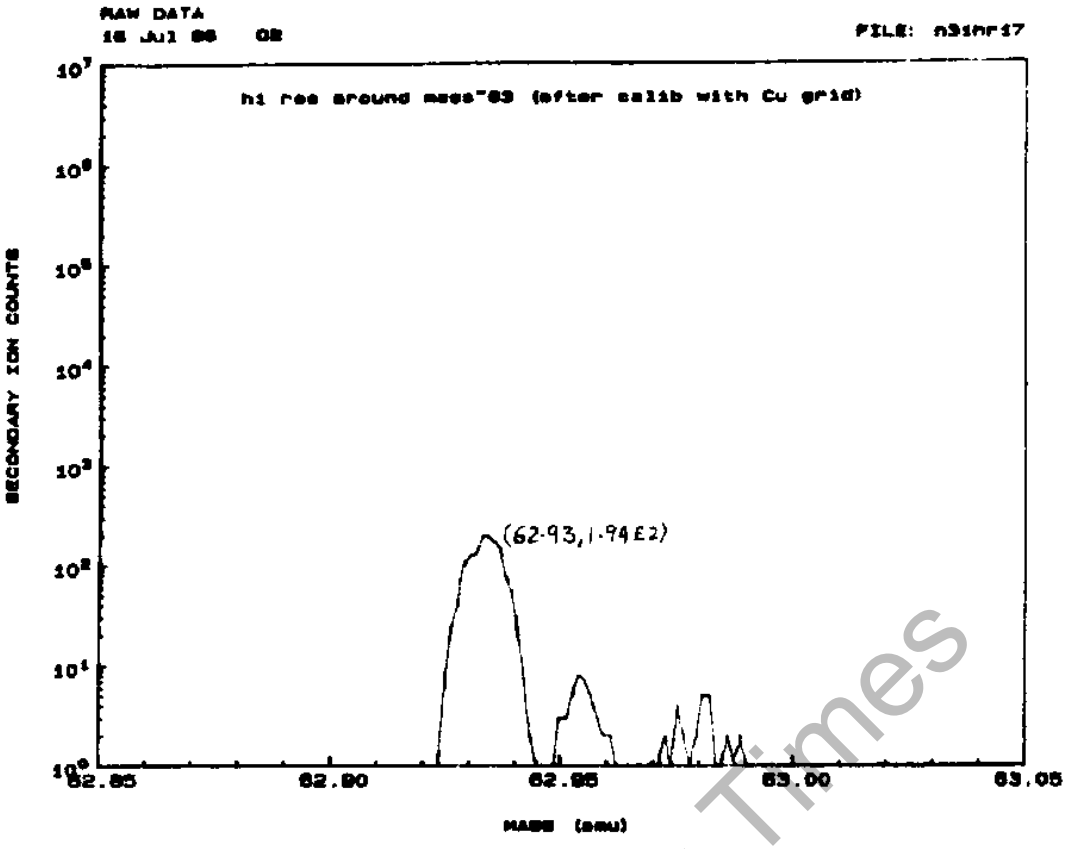

Fig. 3b. High resolution SIMS scan for Cu(63) after the run.

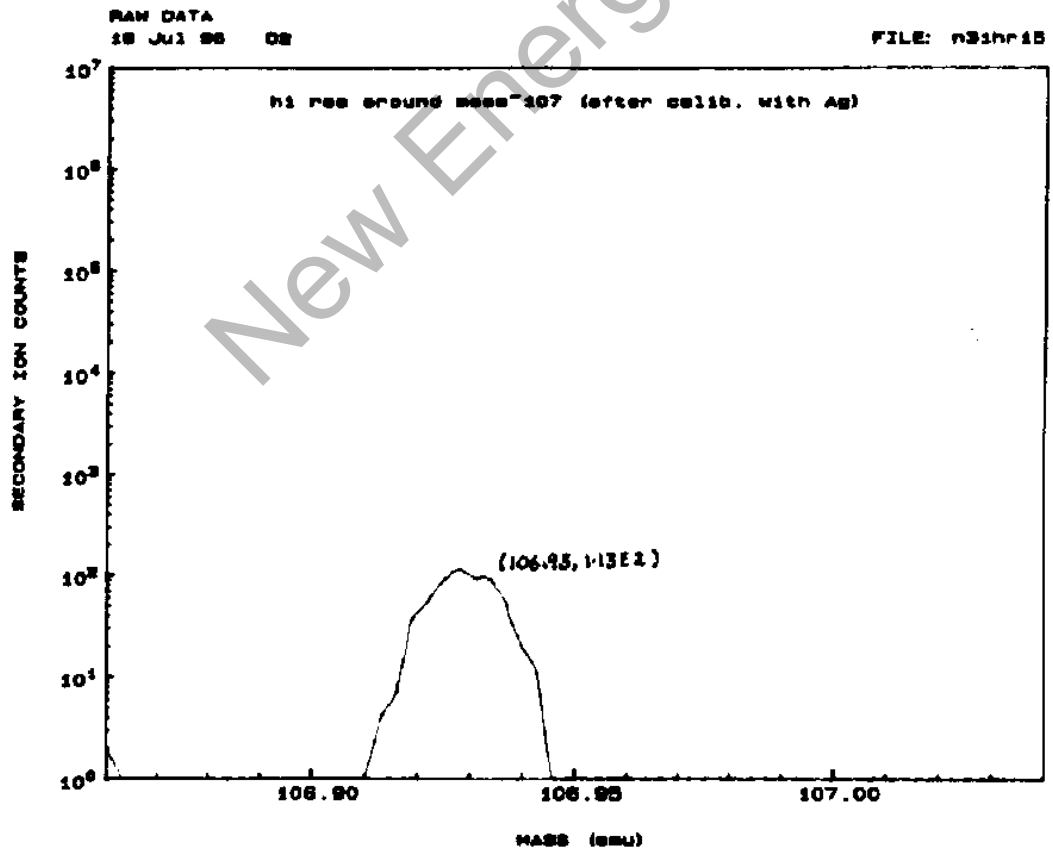

Fig. 3b. High resolution SIMS scan for Ag(107) after the run.

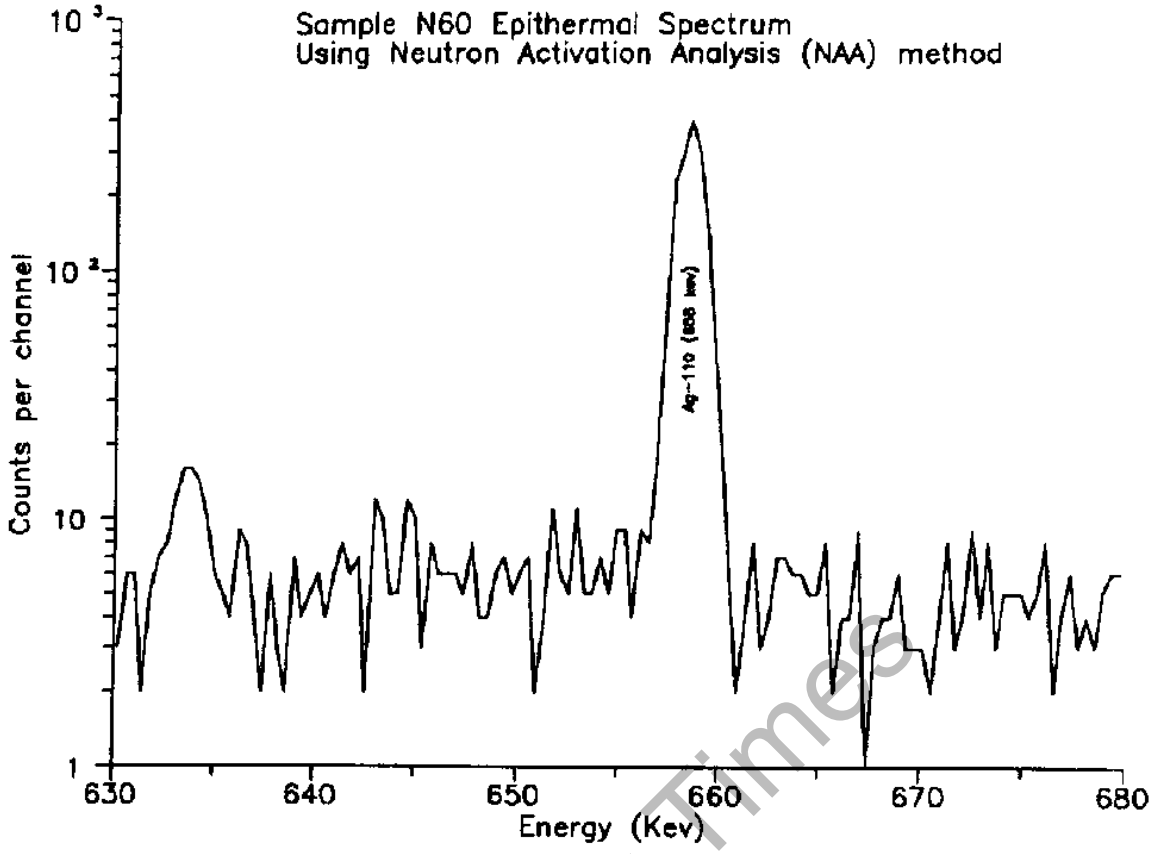

Fig. 4a. Typical NAA gamma spectrum for Ag.

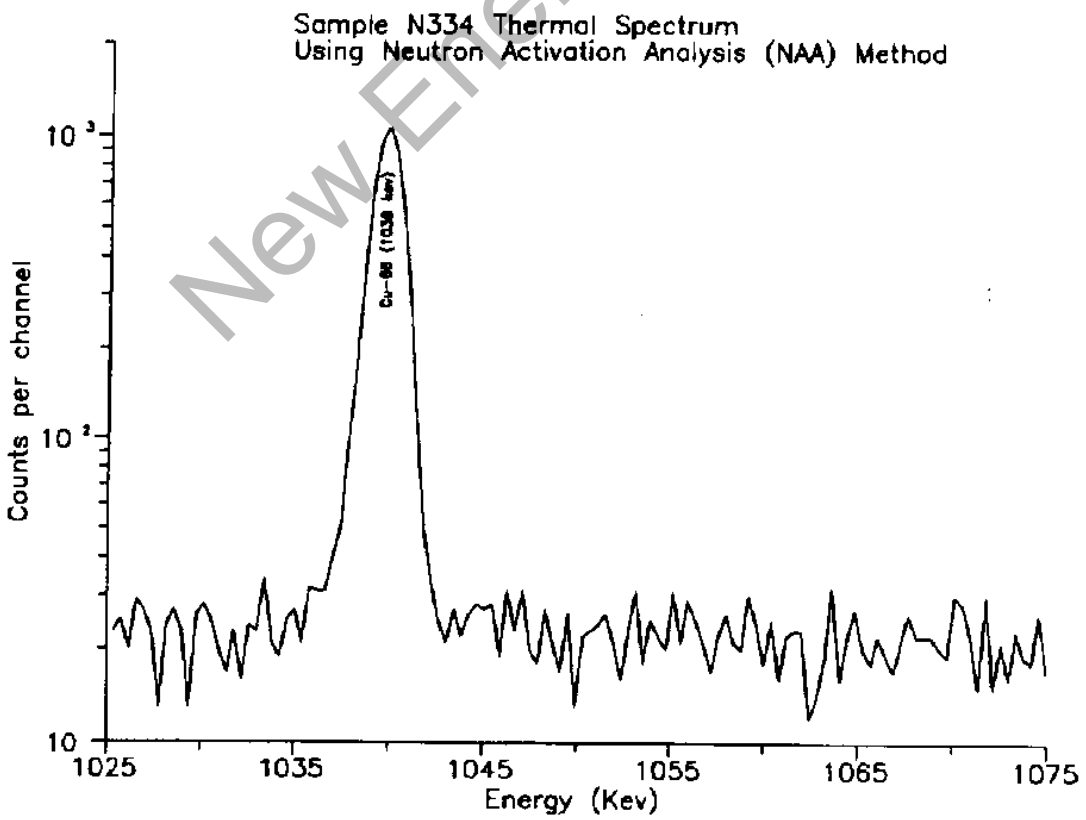

Fig. 4b. NAA gamma spectrum for Cu.

Table 3

Data sheet for change in isotope atom % in metal film after run; comparison to natural abundance (Data from SIMS; isotopes in "bold" use NAA element weight)

Mass No.	Element	Natural a/o	Change (Reacted-Fresh) (in micro-grams)	Fresh MS Atoms	Reacted MS Atoms	Difference % Metal (atomic)	SIMS a/o	Difference in a/o (SIMS-Natural)
28	Si	0.92	1.02E-01	8.14E+16	3.02E+17	1.29E+00	4.67E-01	-45.46
29	Si	0.05	9.80E-03	0.00E+00	2.04E+16	9.79E-01	3.55E-01	30.81
30	Si	0.03	5.07E-03	0.00E+00	1.02E+16	4.89E-01	1.78E-01	14.66
32	S	0.95	9.54E-03	0.00E+00	1.80E+16	8.63E-01	1.00E+00	5.00
45	Sc	1.00	4.45E-05	0.00E+00	5.96E+13	2.87E-03	1.00E+00	0.00
46	Ti	0.08	2.00E-04	0.00E+00	2.62E+14	1.26E-02	4.98E-02	-2.95
47	Ti	0.07	2.79E-04	0.00E+00	3.58E+14	1.72E-02	6.79E-02	-0.49
49	Ti	0.06	2.52E-04	0.00E+00	3.10E+14	1.49E-02	5.88E-02	0.37
50	Ti	0.05	3.60E-03	0.00E+00	4.34E+15	2.08E-01	8.24E-01	77.01
50	**V**	**0.00**	**5.52E-07**	**3.54E+10**	**7.01E+11**	**2.79E-05**	**2.45E-03**	**0.00**
51	**V**	**1.00**	**2.30E-04**	**1.44E+13**	**2.86E+14**	**1.14E-02**	**9.96E-01**	**-0.04**
52	**Cr**	**0.84**	**9.22E-02**	**5.63E+14**	**1.07E+17**	**5.07E+00**	**8.70E-01**	**3.21**
53	**Cr**	**0.10**	**1.19E-02**	**6.27E+13**	**1.36E+16**	**6.42E-01**	**1.10E-01**	**1.51**
54	**Cr**	**0.02**	**2.27E-03**	**1.53E+13**	**2.55E+15**	**1.20E-01**	**2.06E-02**	**-0.30**
54	**Fe**	**0.06**	**1.34E-02**	**2.82E+15**	**1.78E+16**	**3.96E-01**	**5.72E-02**	**-0.10**
55	Mn	1.00	7.30E-02	0.00E+00	8.00E+16	3.85E+00	1.00E+00	0.00
56	**Fe**	**0.92**	**2.11E-01**	**4.29E+16**	**2.70E+17**	**6.01E+00**	**8.69E-01**	**-4.82**
57	**Fe**	**0.02**	**1.24E-02**	**1.01E+15**	**1.41E+16**	**5.14E-01**	**7.42E-02**	**5.23**
59	**Co**	**1.00**	**1.63E-03**	**1.23E+14**	**1.99E+15**	**7.58E-02**	**1.00E+00**	**0.00**
63	**Cu**	**0.69**	**1.17E-01**	**3.57E+15**	**1.16E+17**	**4.99E+00**	**7.00E-01**	**0.80**
64	**Zn**	**0.49**	**1.63E-02**	**1.42E+15**	**1.87E+16**	**5.74E-01**	**3.64E-01**	**-12.47**
65	**Cu**	**0.31**	**5.19E-02**	**1.54E+15**	**4.97E+16**	**2.14E+00**	**3.00E-01**	**-0.80**
66	**Zn**	**0.28**	**9.24E-03**	**7.82E+14**	**9.22E+15**	**3.16E-01**	**2.01E-01**	**-7.72**
67	**Zn**	**0.04**	**2.28E-03**	**1.14E+14**	**2.18E+15**	**8.55E-02**	**5.43E-02**	**1.32**
68	**Zn**	**0.19**	**1.41E-02**	**5.08E+14**	**1.30E+16**	**5.42E-01**	**3.44E-01**	**15.84**
69	Ga	0.60	7.59E-05	0.00E+00	8.64E+13	3.19E-03	5.50E-01	-5.40
70	**Zn**	**0.01**	**1.42E-03**	**1.64E+13**	**1.24E+15**	**5.70E-02**	**3.62E-02**	**3.00**
71	Ga	0.40	6.39E-05	0.00E+00	5.43E+13	2.61E-03	4.50E-01	5.40
72	Ge	0.27	5.39E-03	0.00E+00	4.51E+15	2.17E-01	4.84E-01	21.04
73	Ge	0.08	4.23E-03	0.00E+00	3.49E+15	1.68E-01	3.75E-01	29.74
74	Ge	0.37	8.94E-04	0.00E+00	7.28E+14	3.50E-02	7.81E-02	-28.69
75	As	1.00	4.89E-02	0.00E+00	3.93E+16	1.89E+00	1.00E+00	0.00
76	Ge	0.08	7.34E-04	0.00E+00	5.82E+14	2.80E-02	6.25E-02	-1.51
76	Se	0.09	1.63E-02	0.00E+00	1.29E+16	6.21E-01	1.29E-01	3.88
77	Se	0.08	1.65E-02	0.00E+00	1.29E+16	6.21E-01	1.29E-01	5.32
80	Se	0.50	4.29E-02	0.00E+00	3.23E+16	1.55E+00	3.23E-01	-17.54
82	Se	0.09	5.71E-02	0.00E+00	4.20E+16	2.02E+00	4.19E-01	32.75
85	Rb	0.72	4.03E-07	0.00E+00	2.86E+11	1.37E-05	5.00E-01	-22.20
87	Rb	0.28	4.12E-07	0.00E+00	2.86E+11	1.37E-05	5.00E-01	22.20
87	Sr	0.07	0.00E+00	0.00E+00	0.00E+00	0.00E+00	0.00E+00	-7.02
88	Sr	0.83	2.13E-05	0.00E+00	1.46E+13	7.01E-04	1.00E+00	17.40

Table 3 (continued)

Mass No.	Element	Natural a/o	Change (Reacted-Fresh) (in micro-grams)	Fresh MS Atoms	Reacted MS Atoms	Difference % Metal (atomic)	SIMS a/o	Difference in a/o (SIMS-Natural)
89	Y	1.00	3.37E-05	0.00E+00	2.28E+13	1.10E-03	1.00E+00	0.00
93	Nb	1.00	8.13E-05	0.00E+00	5.27E+13	2.53E-03	1.00E+00	0.00
95	Mo	0.16	1.20E-04	0.00E+00	7.62E+13	3.66E-03	3.33E-01	17.63
96	Zr	0.03	7.85E-05	0.00E+00	4.93E+13	2.37E-03	1.00E+00	97.20
98	Mo	0.24	1.24E-04	0.00E+00	7.62E+13	3.66E-03	3.33E-01	9.53
100	Mo	0.10	1.26E-04	0.00E+00	7.62E+13	3.66E-03	3.33E-01	23.70
107	**Ag**	**0.52**	**1.22E-01**	**7.32E+15**	**7.61E+16**	**2.47E+00**	**5.70E-01**	**5.17**
108	Pd	0.27	3.27E-03	0.00E+00	1.83E+15	8.78E-02	2.73E-01	0.57
109	**Ag**	**0.48**	**9.90E-02**	**6.68E+15**	**6.14E+16**	**1.87E+00**	**4.30E-01**	**-5.17**
110	Pd	0.12	8.89E-03	0.00E+00	4.87E+15	2.34E-01	7.27E-01	60.93
111	Cd	0.13	2.33E-02	0.00E+00	1.27E+16	6.08E-01	1.12E-01	-1.60
112	Cd	0.24	5.38E-02	0.00E+00	2.89E+16	1.39E+00	2.56E-01	1.50
113	Cd	0.12	2.37E-02	0.00E+00	1.27E+16	6.08E-01	1.12E-01	-1.10
113	In	0.04	0.00E+00	0.00E+00	0.00E+00	0.00E+00	0.00E+00	-4.28
114	Cd	0.29	6.33E-02	0.00E+00	3.35E+16	1.61E+00	2.96E-01	0.70
115	In	0.96	4.86E-05	0.00E+00	2.55E+13	1.22E-03	1.00E+00	4.30
116	Cd	0.08	4.87E-02	0.00E+00	2.53E+16	1.22E+00	2.24E-01	14.82
117	Sn	0.08	8.85E-04	0.00E+00	4.56E+14	2.19E-02	1.48E-01	7.20
118	Sn	0.24	2.45E-03	0.00E+00	1.25E+15	6.02E-02	4.07E-01	16.74
119	Sn	0.09	7.87E-04	0.00E+00	3.99E+14	1.92E-02	1.30E-01	4.38
120	Sn	0.33	1.47E-03	0.00E+00	7.41E+14	3.56E-02	2.41E-01	-8.73
121	Sb	0.57	5.05E-03	0.00E+00	2.52E+15	1.21E-01	1.00E+00	42.80
124	Sn	0.06	4.69E-04	0.00E+00	2.28E+14	1.10E-02	7.41E-02	1.47
125	Te	0.07	5.82E-03	0.00E+00	2.81E+15	1.35E-01	3.75E-01	30.51
126	Te	0.19	3.91E-03	0.00E+00	1.87E+15	8.99E-02	2.50E-01	6.30
128	Te	0.32	5.96E-03	0.00E+00	2.81E+15	1.35E-01	3.75E-01	5.70
135	Ba	0.07	5.39E-05	0.00E+00	2.41E+13	1.16E-03	9.26E-02	2.67
137	Ba	0.11	6.93E-05	0.00E+00	3.05E+13	1.47E-03	1.17E-01	0.43
138	Ba	0.72	4.71E-04	0.00E+00	2.06E+14	9.88E-03	7.90E-01	7.31
151	Eu	0.48	1.74E-05	0.00E+00	6.94E+12	3.34E-04	3.33E-01	-14.47
152	Sm	0.27	2.46E-05	0.00E+00	9.74E+12	4.68E-04	2.14E-01	-5.27
153	Eu	0.52	3.52E-05	0.00E+00	1.39E+13	6.67E-04	6.67E-01	14.47
154	Sm	0.23	9.12E-05	0.00E+00	3.57E+13	1.72E-03	7.86E-01	55.87
155	Gd	0.15	3.92E-04	0.00E+00	1.53E+14	7.33E-03	9.09E-01	76.21
156	Gd	0.21	3.95E-05	0.00E+00	1.53E+13	7.33E-04	9.09E-02	-11.41
163	Dy	0.25	2.90E-05	0.00E+00	1.07E+13	5.16E-04	1.00E+00	75.00
165	Ho	1.00	3.42E-05	0.00E+00	1.25E+13	6.00E-04	1.00E+00	0.00
172	Yb	0.22	5.24E-05	0.00E+00	1.83E+13	8.82E-04	1.00E+00	78.20
206	Pb	0.24	2.67E-03	0.00E+00	7.82E+14	3.76E-02	2.67E-01	3.07
207	Pb	0.23	2.69E-03	0.00E+00	7.82E+14	3.76E-02	2.67E-01	4.07
208	Pb	0.52	4.75E-03	0.00E+00	1.37E+15	6.57E-02	4.67E-01	-5.63

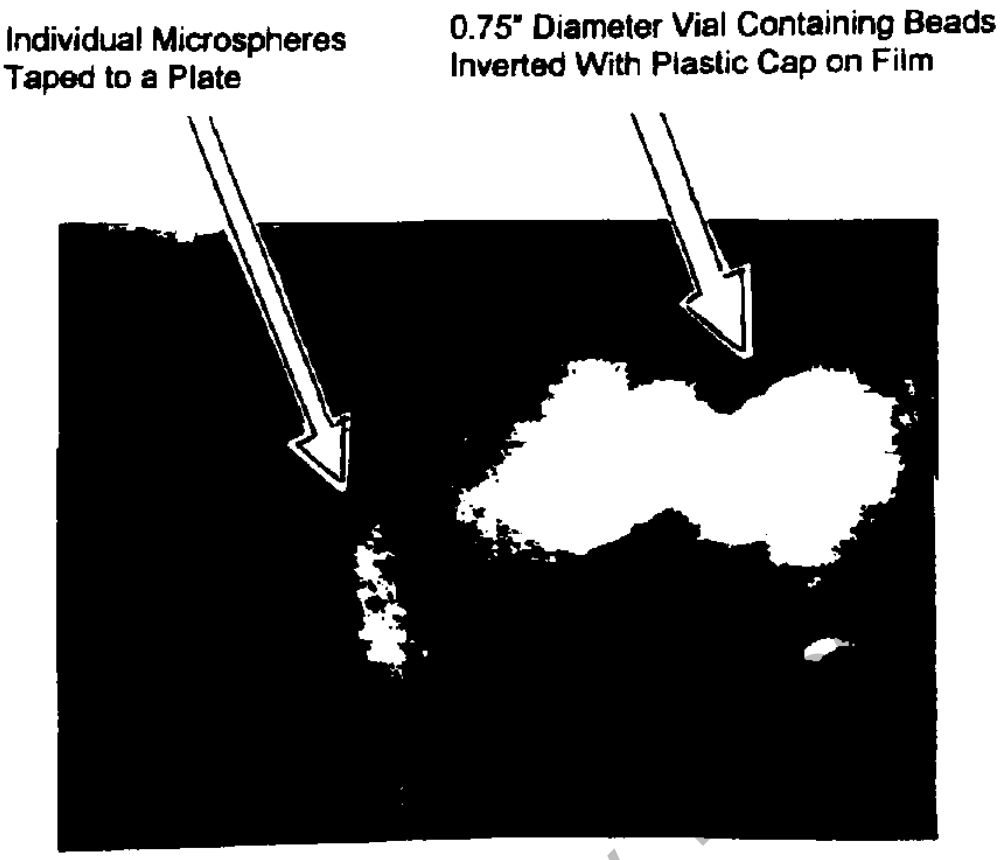

Fig. 6. Nickel microsphere exposure on Kodak ASA 3000 Polaroid film.

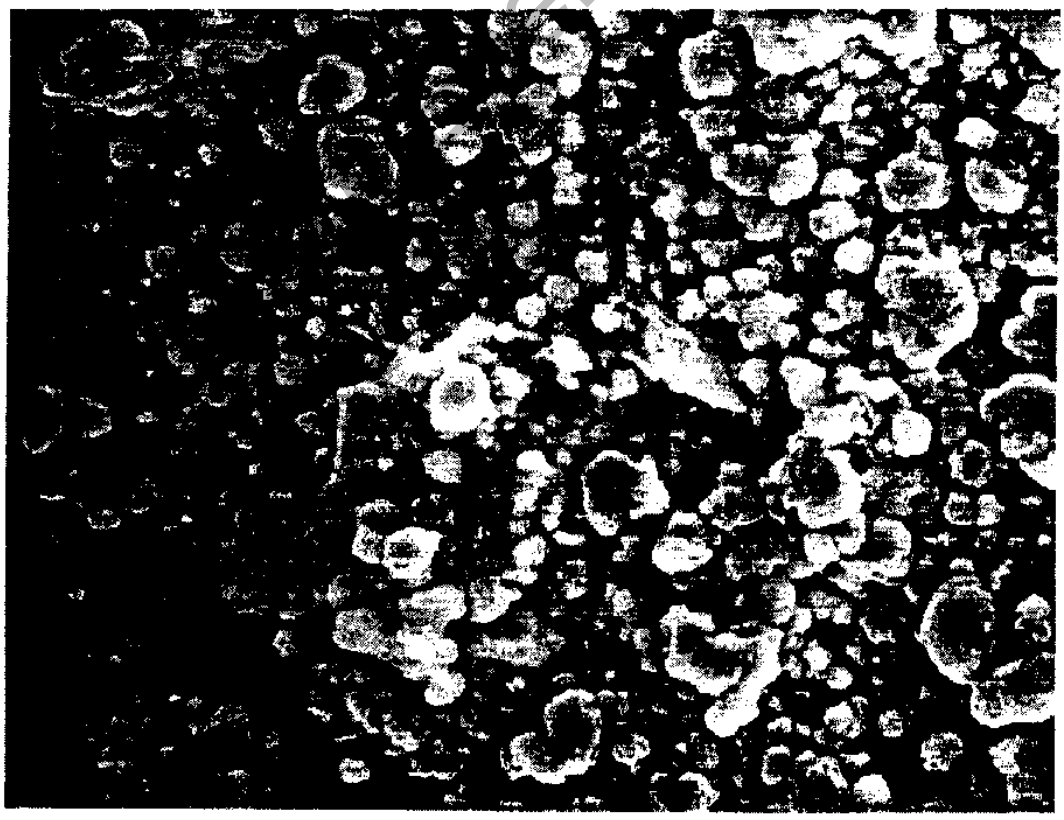

Fig. 7. SEM photograph of debris on filter paper.

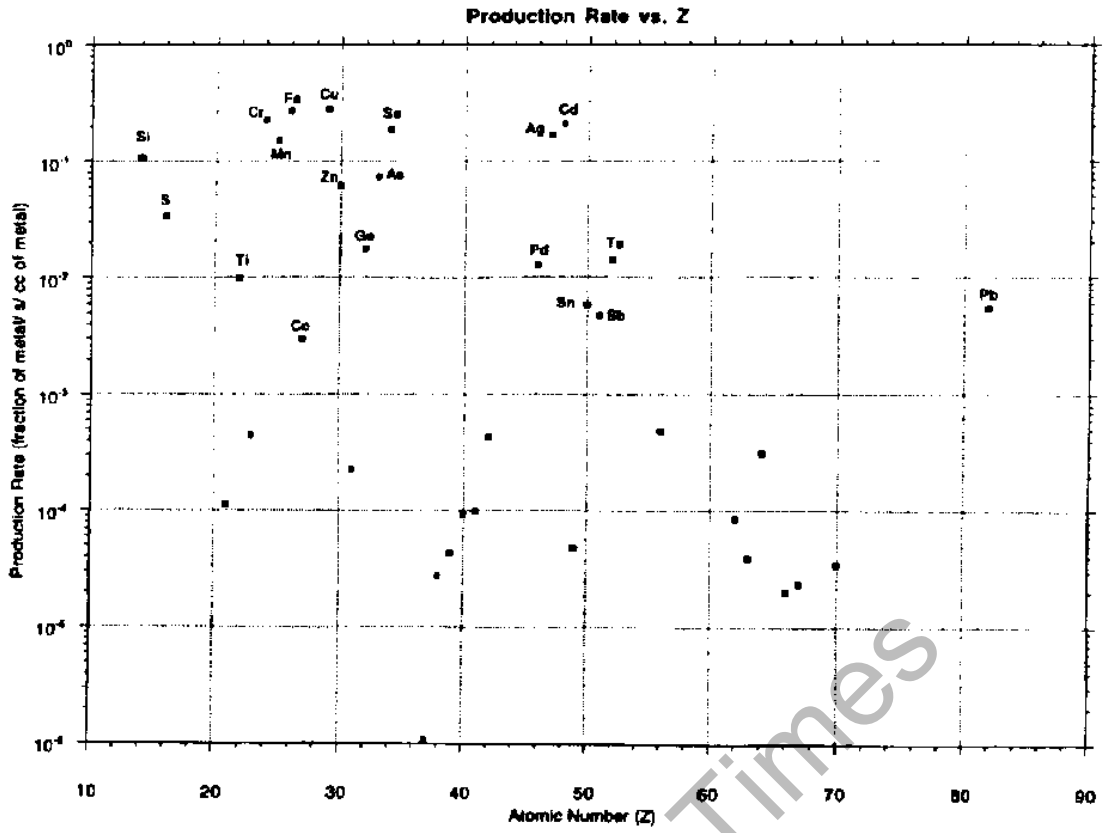

Fig. 8a. Production rate expressed as fraction of metal/ s/ cc of metal vs. atomic number, Z.

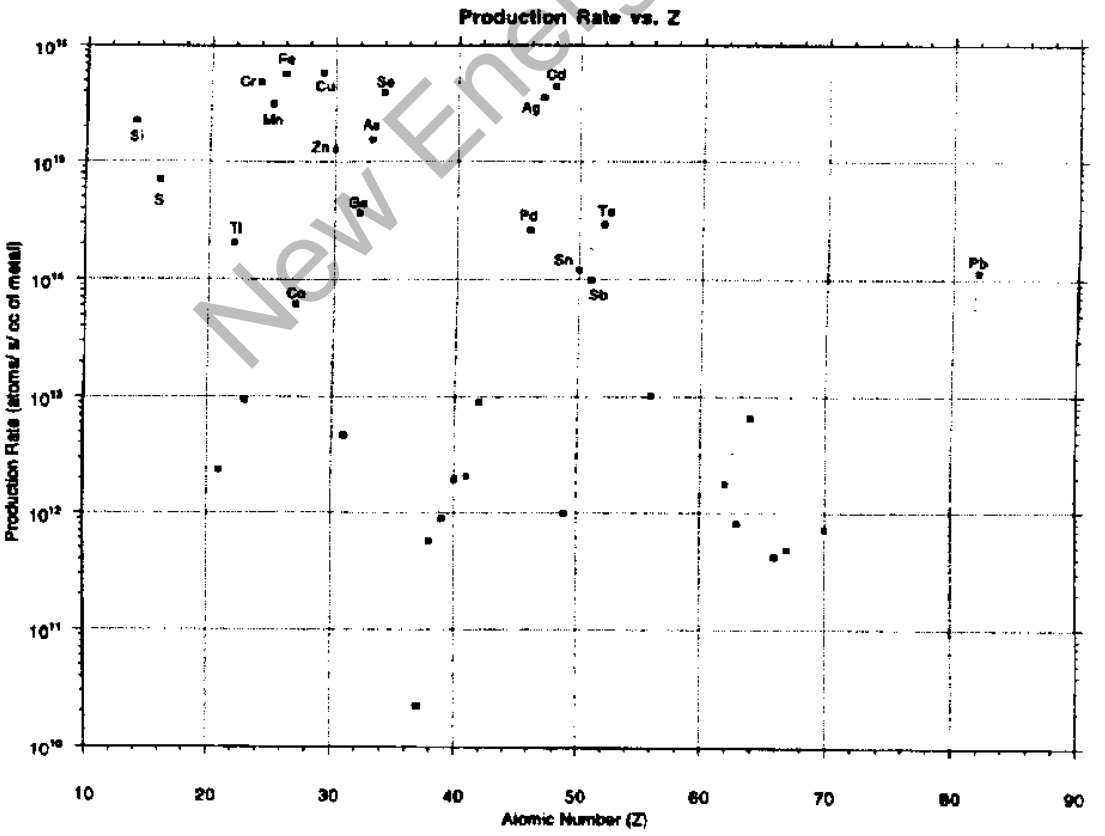

Fig. 8b. Production rate of atoms/ s/ cc of metal vs. atomic number, Z.

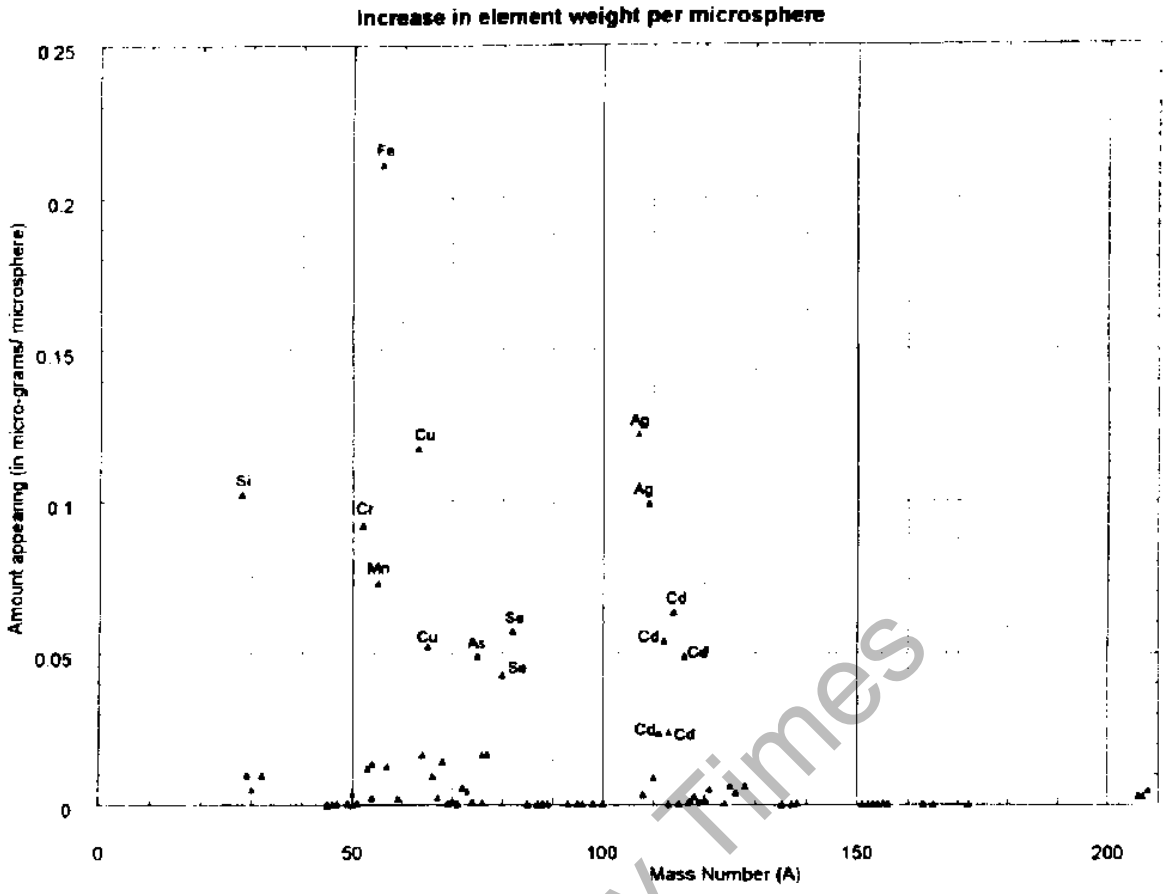

Fig. 9a. Increase in element weight per microsphere.

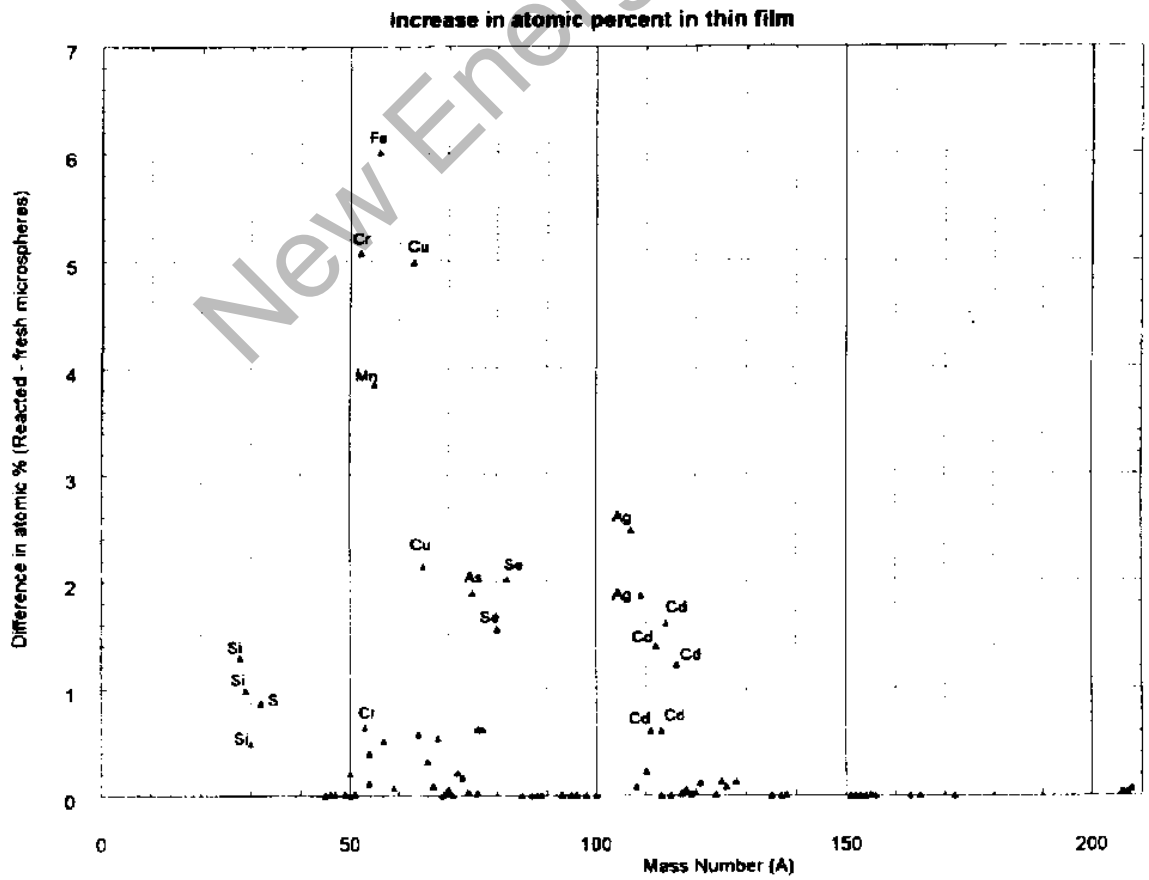

Fig. 9b. Increase in atomic percent in thin film.

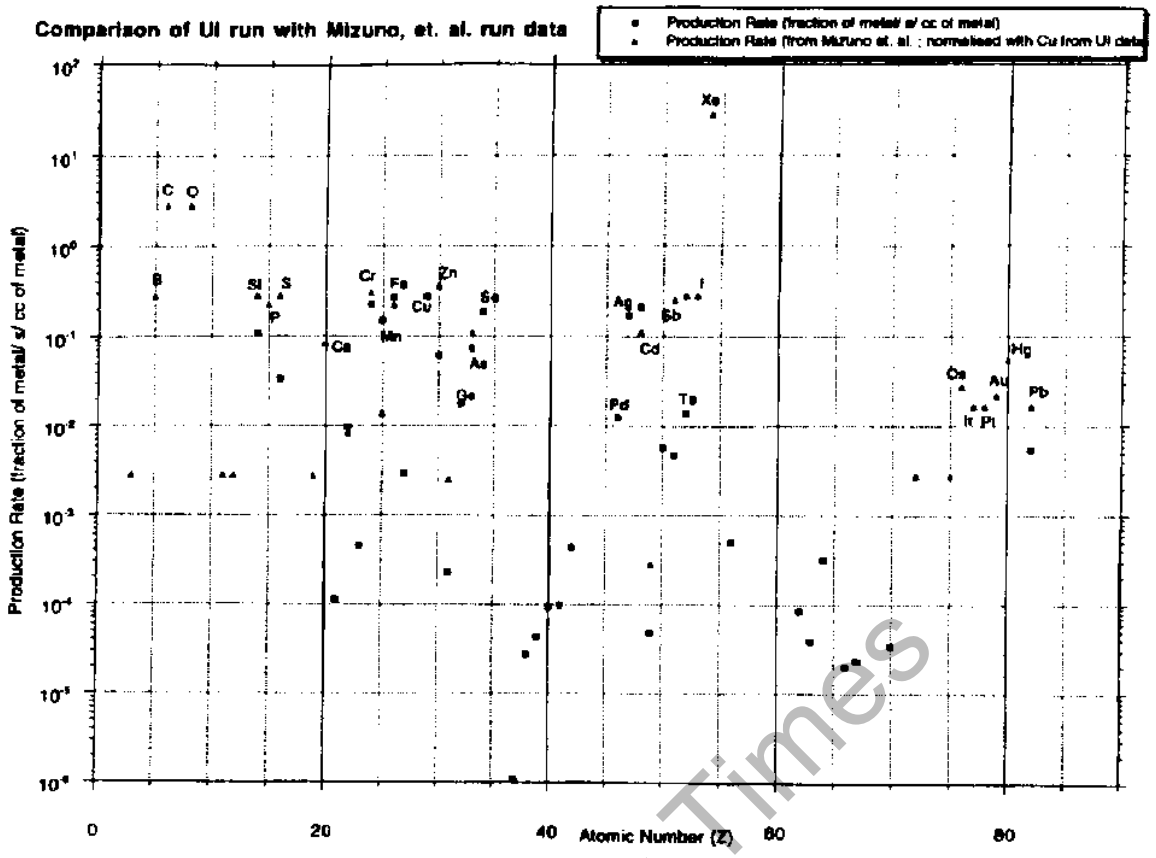

Fig. 10. Comparison of present production rate data with Mizuno et al.

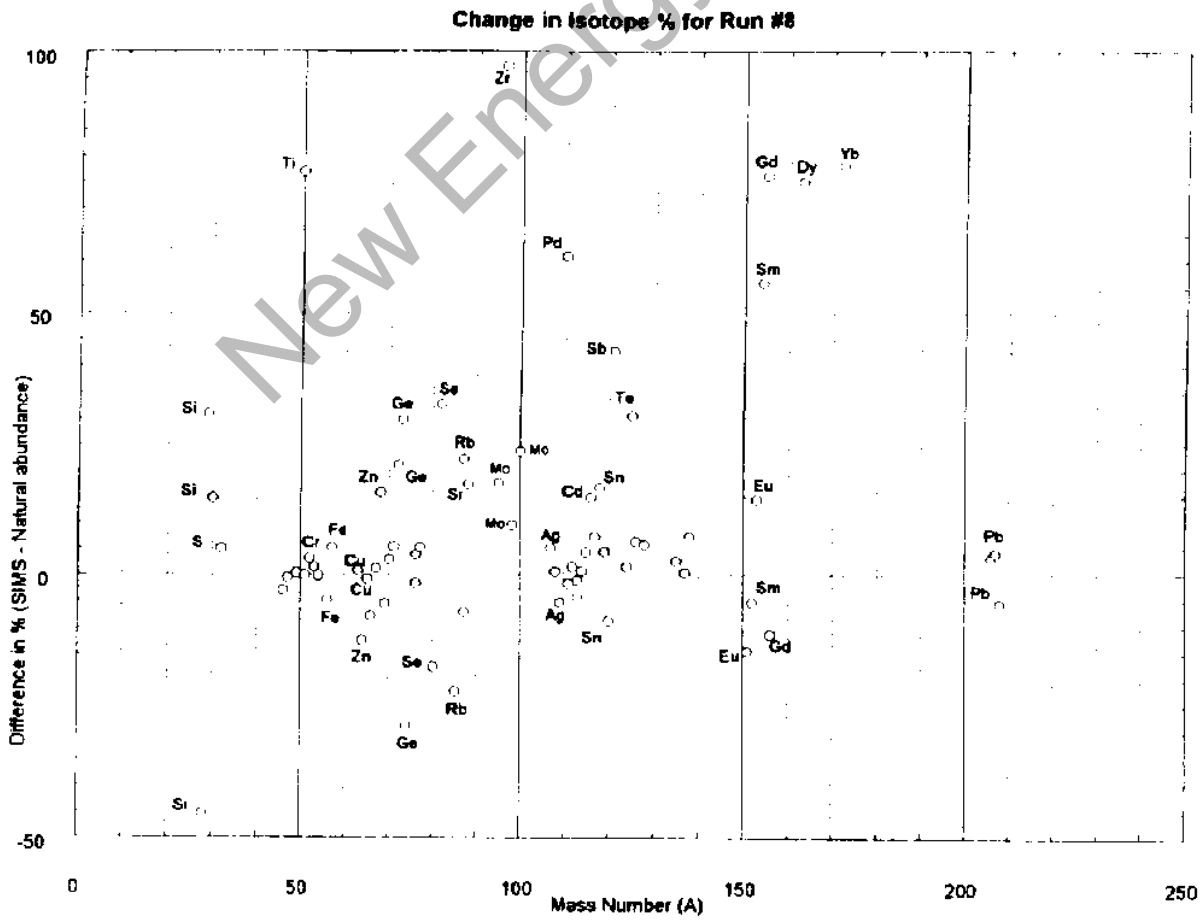

Fig. 11. Isotope shifts (percent SIMS - percent natural abundance) vs. mass number, A.